A Simple Representation of Three-Dimensional Molecular Structure

Seth D. Axen,[†] Xi-Ping Huang,[‡,∥] Elena L. Cáceres,[†,§] Leo Gendelev,[†,§] Bryan L. Roth,[‡,∥,⊥] and Michael J. Keiser*[,†,§]

[†]Department of Bioengineering and Therapeutic Sciences, University of California, San Francisco, 675 Nelson Rising Lane NS 416A, San Francisco, California 94143, United States

[‡]Department of Pharmacology, University of North Carolina School of Medicine, Chapel Hill, North Carolina 27599, United States

[§]Department of Pharmaceutical Chemistry, Institute for Neurodegenerative Diseases, and Institute for Computational Health Sciences, University of California, San Francisco, 675 Nelson Rising Lane NS 416A, San Francisco, California 94143, United States

[∥]National Institute of Mental Health Psychoactive Drug Screening Program (NIMH PDSP), University of North Carolina, Chapel Hill, North Carolina 27599, United States

[⊥]Division of Chemical Biology and Medicinal Chemistry, Eshelman School of Pharmacy, University of North Carolina at Chapel Hill, Chapel Hill, North Carolina 27599, United States

Ⓢ *Supporting Information*

ABSTRACT: Statistical and machine learning approaches predict drug-to-target relationships from 2D small-molecule topology patterns. One might expect 3D information to improve these calculations. Here we apply the logic of the extended connectivity fingerprint (ECFP) to develop a rapid, alignment-invariant 3D representation of molecular conformers, the extended three-dimensional fingerprint (E3FP). By integrating E3FP with the similarity ensemble approach (SEA), we achieve higher precision-recall performance relative to SEA with ECFP on ChEMBL20 and equivalent receiver operating characteristic performance. We identify classes of molecules for which E3FP is a better predictor of similarity in bioactivity than is ECFP. Finally, we report novel drug-to-target binding predictions inaccessible by 2D fingerprints and confirm three of them experimentally with ligand efficiencies from 0.442−0.637 kcal/mol/heavy atom.
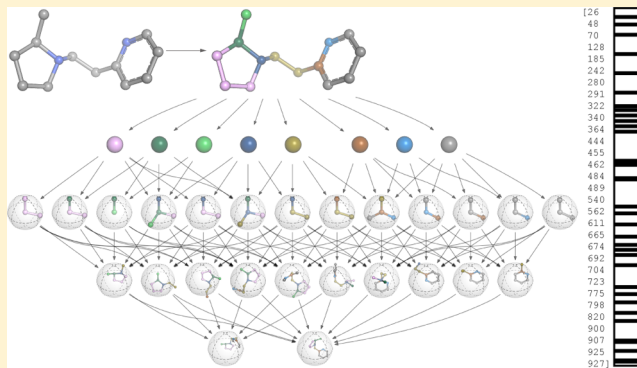
INTRODUCTION

Many molecular representations have arisen since the early chemical informatics models of the 1970s, yet the most widely used still operate on the simple two-dimensional (topological) structures of small molecules. Fingerprints, which encode molecular 2D substructures as overlapping lists of patterns, were a first means to scan chemical databases for structural similarity using rapid bitwise logic on pairs of molecules. Pairs of molecules that are structurally similar, in turn, often share bioactivity properties[1] such as protein binding profiles. Whereas the prediction of biological targets for small molecules would seem to benefit from a more thorough treatment of a molecule's explicit ensemble of three-dimensional (3D) conformations,[2] pragmatic considerations such as calculation cost, alignment invariance, and uncertainty in conformer prediction[3] nonetheless limit the use of 3D representations by large-scale similarity methods such as the similarity ensemble approach (SEA),[4,5] wherein the count of pairwise molecular calculations reaches into the hundreds of billions. Furthermore, although 3D representations might be expected to outperform 2D ones, in practice, 2D

representations nonetheless are in wider use and can match or outperform them.[3,6−8]

The success of statistical and machine learning approaches building on 2D fingerprints reinforces the trend. Naive Bayes classifiers (NB),[9−11] random forests (RF),[12,13] support vector machines (SVM),[9,14,15] and deep neural networks (DNN)[16−20] predict a molecule's target binding profile and other properties from the features encoded into its 2D fingerprint. SEA and methods building on it such as optimized cross reactivity estimation (OCEAN)[21] quantify and statistically aggregate patterns of molecular pairwise similarity to the same ends. Yet these approaches cannot readily be applied to the 3D molecular representations most commonly used. The rapid overlay of chemical structures (ROCS) method is an alternative to fingerprints that instead represents molecular shape on a conformer-by-conformer basis via Gaussian functions centered on each atom. These functions may then be compared between a pair of conformers.[22,23] ROCS, however, must align conformers
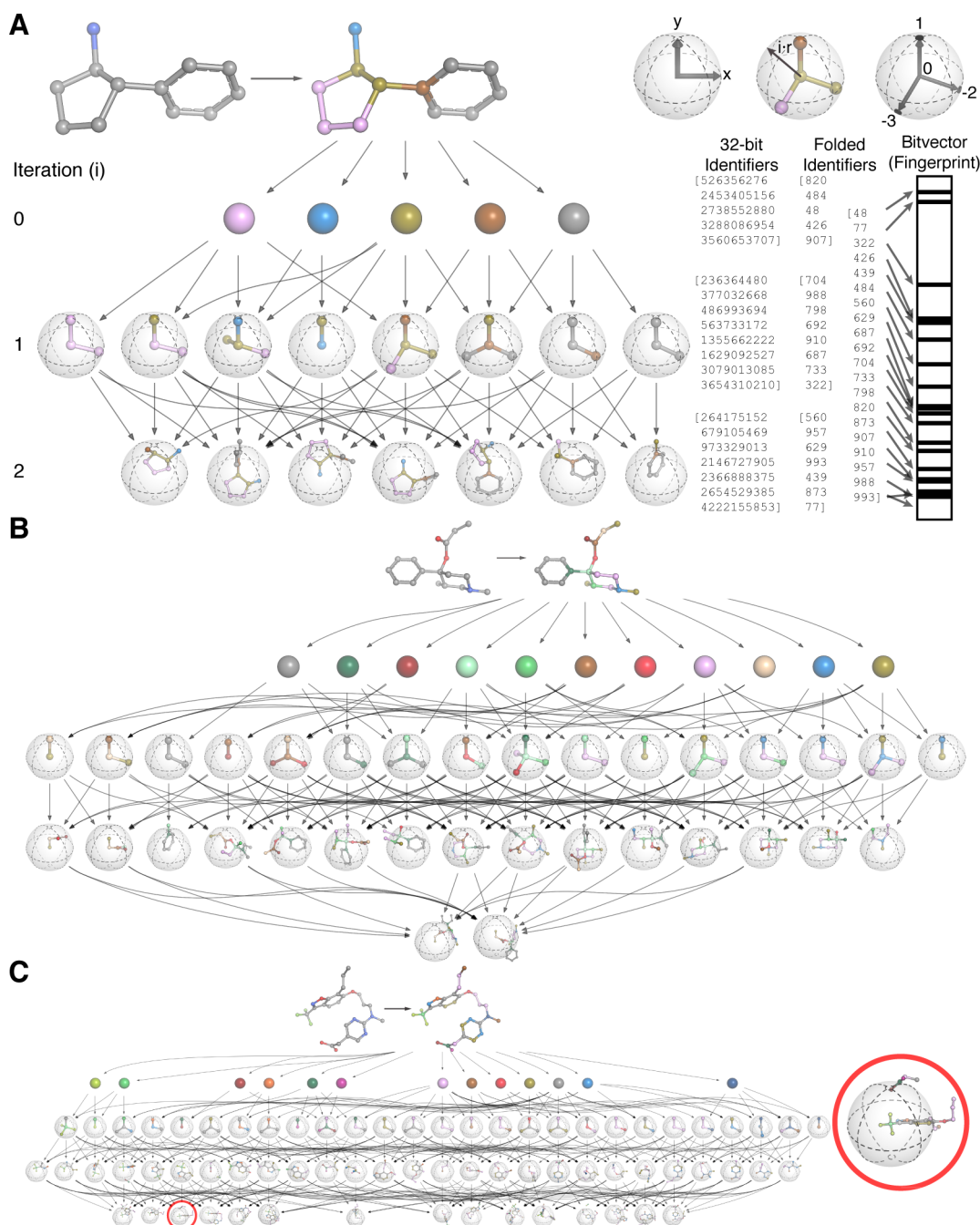
Figure 1. Diagram of information flow in the E3FP algorithm. (A) Overview of fingerprinting process for cypenamine. At iteration 0, we assign atom identifiers using a list of atomic invariants and hash these into integers (shown here also as unique atom colors). At iteration i, shells of radius $i \cdot r$ center on each atom (top right). The shell contains bound and unbound neighbor atoms. Where possible, we uniquely align neighbor atoms to the xy-plane (top right) and assign stereochemical identifiers. Convergence occurs when a shell's substructure contains the entire molecule (third from the right) or at the maximum iteration count. Finally we "fold" each iteration's substructure identifiers to 1024-bit space. (B) Overview of fingerprinting for alphaprodine. (C) Overview of fingerprinting for a large, flexible molecule (CHEMBL210990; expanded in Supporting Information, Figure S1). A three-dimensional substructure can consist of two disconnected substructures and their relative orientations (right).

to determine pairwise similarity; in addition to the computational cost of each alignment, which linear algebraic approximations such as SCISSORS[24] mitigate, the method provides no invariant fixed-length fingerprint (feature vectors) per molecule or per conformer for use in machine learning. One way around this limitation is to calculate an all-by-all conformer similarity matrix ahead of time, but this is untenable for large data sets such as ChEMBL[25] or the 70-million data point ExCAPE-DB,[26] especially as the data sets continue to grow.

Feature point pharmacophores (FEPOPS), on the other hand, use k-means clustering to build a fuzzy representation of a conformer using a small number of clustered atomic feature points, which simplify shape and enable rapid comparison.[27,28] FEPOPS excels at scaffold hopping, and it can use charge-distribution-based prealignment to circumvent a pairwise alignment step. However, prealignment can introduce similarity artifacts such that explicit pairwise shape-based or feature-point-based alignment may nonetheless be preferred.[27] Accordingly,

3D molecular representations and scoring methods typically align conformers on a pairwise basis.[2,3] Another promising method, torsion fingerprint deviation (TFD), requires a preliminary atom mapping between molecules to ensure comparison of the correct torsion angles.[29] An alternative approach is to encode conformers against 3- or 4-point pharmacophore keys that express up to 890 thousand or 350 million discrete pharmacophores, respectively.[30,31] The count of purchasable molecules alone, much less their conformers, however, exceeds 200 million in databases such as ZINC (zinc.docking.org),[32] and the structural differences determining bioactivity may be subtle. Atom-pair fingerprints are one potentially more scalable approach, with natural implementations in 2D and 3D amenable to comparison.[33,34]

To directly integrate 3D molecular representations with statistical and machine learning methods, we developed a 3D fingerprint that retains the advantages of 2D topological fingerprints. Inspired by the widely used circular ECFP (2D) fingerprint, we develop a spherical extended 3D fingerprint (E3FP) and assess its performance relative to ECFP for various systems pharmacology tasks. E3FP is an open-source fingerprint that encodes 3D information without the need for molecular alignment, scales linearly with 2D fingerprint pairwise comparisons in computation time, and is compatible with statistical and machine learning approaches that have already been developed for 2D fingerprints. We use it to elucidate regions of molecular similarity space that could not previously be explored. To demonstrate its utility, we combine E3FP with SEA to predict novel target-to-drug activities that SEA could not discover using ECFP and confirm experimentally that they are correct.

■ RESULTS

The three-dimensional fingerprints we present are motivated by the widely used two-dimensional (2D) extended connectivity fingerprint (ECFP),[35] which is based on the Morgan algorithm.[36] ECFP is considered a 2D or "topological" approach because it encodes the internal graph connectivity of a molecule without explicitly accounting for 3D structural patterns the molecule may adopt in solution or during protein binding. While ECFP thus derives from the neighborhoods of atoms directly connected to each atom, a 3D fingerprint could incorporate neighborhoods of nearby atoms in 3D space, even if they are not directly bonded. We develop such an approach and call it an extended three-dimensional fingerprint (E3FP).

A Single Small Molecule Yields Multiple 3D Fingerprints. Many small molecules can adopt a number of energetically favorable 3D conformations, termed "conformers". In the absence of solved structures, it is not always apparent which conformer a molecule will adopt in solution, how this may change on protein binding, and which protein−ligand interactions may favor which conformers.[37] Accordingly, we generate separate E3FPs for each of multiple potential conformers per molecule. E3FP encodes all three-dimensional substructures from a single conformer into a bit vector, represented as a fixed-length sequence of 1s and 0s (Figure 1A). This is analogous to the means by which ECFPs represent two-dimensional substructures. To encode the three-dimensional environment of an atom, E3FP considers information pertaining not only to contiguously bound atoms but also to nearby unbound atoms and to relative atom orientations (stereochemistry). We designed this process to be minimally sensitive to minor structural fluctuations so that conformers could be distinguished while the set of conformers for a given

molecule would retain a degree of internal similarity in E3FP space.

The binding-relevant conformers of most small molecules are not known a priori. Accordingly, prior to constructing any 3D fingerprint, we generate a library of potential conformers for the molecule, each of which in turn will have a unique fingerprint. We employed a previously published protocol using the open-source RDKit package,[38] wherein the authors determined the number of conformers needed to recover the correct ligand conformation from a crystal structure as a function of the number of rotatable bonds in the molecule, with some tuning (see Experimental Section).

E3FP Encodes Small-Molecule 3D Substructures. The core intuition of E3FP generation (Figure 1A) is to draw concentrically larger shells and encode the 3D atom neighborhood patterns within each of them. To do so, the algorithm proceeds from small to larger shells iteratively. First, as in ECFP, we uniquely represent each type of atom and the most important properties of its immediate environment. To do so, we assign 32-bit integer identifiers to each atom unique to its count of heavy atom immediate neighbors, its valence minus neighboring hydrogens, its atomic number, its atomic mass, its atomic charge, its number of bound hydrogens, and whether it is in a ring. This can result in many fine-grained identifiers, some examples of which are visualized as differently colored atoms for the molecule cypenamine in Figure 1A and for larger molecules in Figure 1B,C.

At each subsequent iteration, we draw a shell of increasing radius around each atom, defining the neighbors as the atoms within the shell as described above. The orientation and connectivity of the neighbors, or lack thereof (as in Figure 1C, red circle, expanded in Supporting Information (SI), Figure S1), is combined with the neighbors' own identifiers from the previous iteration to generate a new joint identifier. Thus, at any given iteration, the information contained within the shell is the union of the substructures around the neighbors from the previous iterations merged with the neighbors' orientation and connectivity with respect to the center atom of the current shell. The set of atoms represented by an identifier therefore comprise a three-dimensional substructure of the molecule.

We continue this process up to a predefined maximum number of iterations or until we have encountered all substructures possible within that molecule. We then represent each identifier as an "on" bit in a sparse bit vector representation of the entire conformer (Figure 1A, bitvector). Each "on" bit indicates the presence of a specific three-dimensional substructure. The choice of numerical integer to represent any identifier is the result of a hash function (see Experimental Section) that spreads the identifiers evenly over a large integer space. Because there are over four billion possible 32-bit integers and we observe far fewer than this number of molecular substructures (identifiers) in practice, each identifier is unlikely to collide with another and may be considered unique to a single atom or substructure. Because this still remains a mostly empty identifier space, we followed the commonly used approach from ECFP and "fold" E3FP down to a shorter bitvector for efficient storage and swift comparison, adapting the 1024-bit length that has been effective for ECFP4[6,39] (SI, Table S2).

To demonstrate the fingerprinting process, Figure 1A steps through the generation of an E3FP for the small molecule cypenamine. First, four carbon atom types and one nitrogen atom type are identified, represented by five colors. As cypenamine is fairly small, E3FP fingerprinting terminates after two iterations, at which point one of the substructures consists of
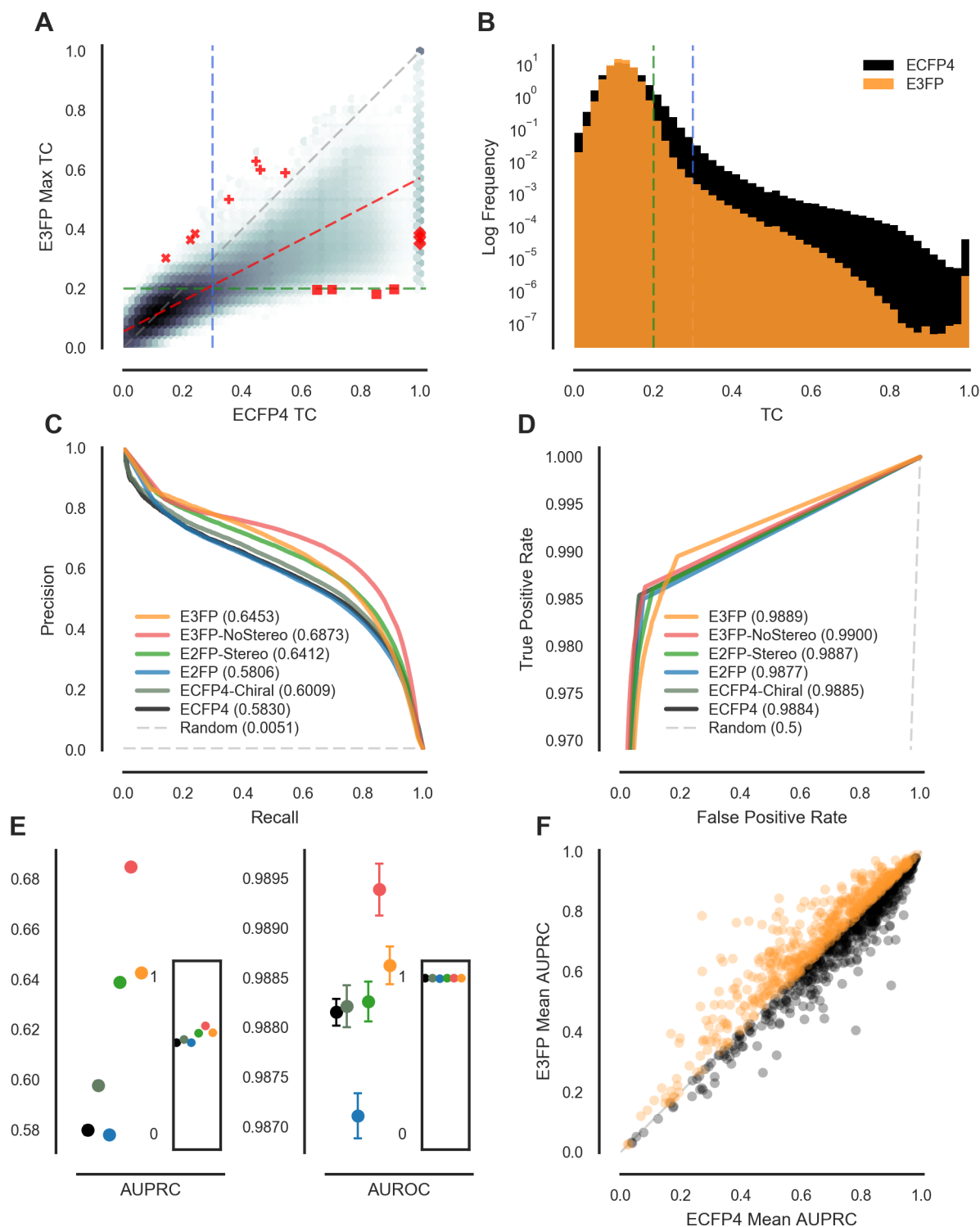
Figure 2. Comparative performance of E3FP and ECFP4. For all pairs of 308315 molecules from ChEMBL20, (A) log density plot summarizing 48 billion maximum Tanimoto coefficients (TC) calculated between E3FP conformer fingerprint sets versus corresponding TC by ECFP4 fingerprints. The dotted red line is a linear least-squares fit. Optimal SEA TC cutoffs for E3FP (green) and ECFP4 (blue) are dotted lines. Red markers indicate examples in Figure 3. (B) Histograms of TCs from (A). (C) Combined precision-recall (PRC) curves from five independent 5-fold cross-validation runs using 1024-bit E3FP, E3FP without stereochemical identifiers (E3FP-NoStereo), E3FP without stereochemical identifiers or nearby unbound atoms (E2FP), E3FP without nearby unbound atoms (E2FP-Stereo), ECFP4, and ECFP4 with distinct bond types encoding chirality (ECFP4-Chiral). Only the PRC of the highest AUC fold is shown. (D) Combined highest-AUC ROC curves for the same sets as in (C). (E) Results of bootstrapping AUCs as in Table 1. Dots indicate mean AUC, and whiskers standard deviations. Insets show absolute scale. (F) Target-wise comparison of mean AUPRCs using E3FP versus ECFP4.

the entire molecule. The slightly larger molecule alphaprodine takes an additional iteration to reach termination (Figure 1B).

Figure 1C and SI, Figure S1, demonstrate the same process for CHEMBL210990.[25] This molecule is more complex, with 13

Table 1. Performance of Variants of E3FP and ECFP Using SEA[a]

name	mean fold AUPRC	mean fold AUROC	mean target AUPRC	mean target AUROC
ECFP4	0.5799 ± 0.0018	0.9882 ± 0.0001	0.6965 ± 0.2099	0.9772 ± 0.0387
ECFP4-Chiral	0.5977 ± 0.0017	0.9882 ± 0.0002	0.7021 ± 0.2088	0.9769 ± 0.0391
E2FP	0.5781 ± 0.0015	0.9871 ± 0.0002	0.7080 ± 0.2034	0.9768 ± 0.0392
E2FP-Stereo	0.6390 ± 0.0011	0.9883 ± 0.0001	0.7140 ± 0.2016	0.9780 ± 0.0371
E3FP-NoStereo	**0.6849 ± 0.0012**	**0.9894 ± 0.0003**	**0.7312 ± 0.1989**	0.9774 ± 0.0409
E3FP	0.6426 ± 0.0016	0.9886 ± 0.0002	0.7046 ± 0.1991	**0.9805 ± 0.0326**
E3FP-RDKit	0.6409 ± 0.0014	0.9885 ± 0.0003	0.7086 ± 0.2003	0.9798 ± 0.0348

[a]Mean and standard deviations for combined fold AUPRC and AUROC curves versus target-wise AUPRC and AUROC curves across five independent repeats of 5-fold cross-validation are shown. A random classifier will produce a mean AUPRC of 0.0051 (fraction of positive target/mol pairs in test data), a mean target AUPRC of 0.0053 ± 0.0076, and a mean AUROC and mean target-wise AUROC of 0.5.

distinct atom types, and in the conformation shown reaches convergence in three iterations. Because the molecule bends back on itself, in the second and third iterations, several of the identifiers represent substructures that are nearby each other in physical space but are not directly bound to each other and indeed are separated by many bonds (e.g., red circle in Figure 1C). 2D fingerprints such as ECFP are inherently unaware of unconnected proximity-based substructures, but they are encoded in E3FP.

SEA 3D Fingerprint Performance Exceeds That of 2D in Binding Prediction. We were curious to determine how molecular similarity calculations using the new E3FP representations would compare to those using the 2D but otherwise similarly motivated ECFP fingerprints. Specifically, we investigated whether the 3D fingerprint encoded information that would enhance performance over its 2D counterpart in common chemical informatics tasks.

The ECFP approach uses several parameters (e.g., ECFP4 uses a radius of 2), and prior studies have explored their optimization.[39] We likewise sought appropriate parameter choices for E3FP. In addition to the conformer generation choices described above, E3FP itself has four tunable parameters: (1) a shell radius multiplier (r in Figure 1A), (2) number of iterations (i in Figure 1A), (3) inclusion of stereochemical information, and (4) final bitvector length (1024 in Figure 1A). We explored which combinations of conformer generation and E3FP parameters produced the most effective 3D fingerprints for the task of recovering correct ligand binders for over 2000 protein targets using the similarity ensemble approach (SEA). SEA compares sets of fingerprints against each other using Tanimoto coefficients (TC) and determines a *p-value* for the similarity among the two sets; it has been used to predict drug off-targets,[4,5,40,41] small-molecule mechanisms of action,[42−44] and adverse drug reactions.[4,45,46] For the training library, we assembled a data set of small-molecule ligands that bind to at least one of the targets from the ChEMBL database with an IC$_{50}$ of 10 μM or better. We then generated and fingerprinted the conformers using each E3FP parameter choice, resulting in a set of conformer fingerprints for each molecule and for each target. We performed a stratified 5-fold cross-validation on a target-by-target basis by setting aside one-fifth of the known binders from a target for testing, searching this one-fifth (positive data) and the remaining nonbinders (negative data) against the target using SEA, and then computing true and false positive rates at all possible SEA *p-value* cutoffs. For each target in each fold, we computed the precision recall curve (PRC), the receiver operating characteristic (ROC), and the area under each curve (AUC). Likewise, we combined the predictions across all targets in a cross-validation fold to generate fold PRC and ROC curves.

As there are far more negative target−molecule pairs in the test sets than positives, a good ROC curve was readily achieved, as many false positives must be generated to produce a high false positive rate. Conversely, in such a case, the precision would be very low. We therefore expected the AUC of the PRC (AUPRC) to be a better assessment of parameter set.[47] To simultaneously optimize for both a high AUPRC and a high AUC of the ROC (AUROC), we used the sum of these two values as the objective function, AUC$_{SUM}$. We employed the Bayesian optimization program Spearmint[48] to optimize four of five possible E3FP parameters (we did not optimize fingerprint bit length, for simplicity of comparison to ECFP fingerprints) so as to maximize the AUC$_{SUM}$ value and minimize runtime of fingerprinting (SI, Figure S2).

We constrained all optimization solely to the choice of fingerprint parameters on the same underlying collection of precomputed molecular conformers. For computational efficiency, we split the optimization protocol into two stages (see Experimental Section). This yielded an E3FP parameter set that used the three lowest energy conformers, a shell radius multiplier of 1.718, and five iterations of fingerprinting (SI, Figure S4). After bootstrapping with five independent repeats of 5-fold cross-validation using E3FP and ECFP4 on a larger set of 308315 ligands from ChEMBL20, E3FP produced a mean AUPRC of 0.6426, exceeding ECFP4's mean AUPRC of 0.5799 in the same task (Figure 2C,E, Table 1). Additionally, E3FP's mean AUROC of 0.9886 exceeds ECFP4's AUPRC of 0.9882 (Figure 2D,E, Table 1). Thus, at a SEA *p-value* threshold $p \leq 3.45 \times 10^{-47}$, E3FP achieves an average *sensitivity* of 0.6976, *specificity* of 0.9974, *precision* of 0.5824, and F_1 score of 0.6348. ECFP4 achieves 0.4647, 0.9986, 0.6236, and 0.5325, at this *p-value* threshold. ECFP4 is unable to achieve the high F_1 score of E3FP, but at its maximum F_1 score of 0.5896, it achieves a *sensitivity* of 0.6930, a *specificity* of 0.9966, and a *precision* of 0.5131 using a *p-value* threshold $p \leq 3.33 \times 10^{-23}$. To ensure a fair comparison, we subjected ECFP to a grid search on its radius parameter and found that no radius value outperforms ECFP4 with both AUPRC and AUROC (SI, Table S1). Additionally, fingerprints with longer bit lengths did not yield significant performance increases for E3FP or ECFP4 despite the expectation that longer lengths would lower feature collision rates (SI, Table S2); indeed, it appears that increasing the fingerprint length reduced the performance of E3FP. RDKit uses slightly different atomic invariants for its Morgan fingerprints than E3FP's default Daylight invariants, but we found that RDKit's invariants with E3FP ("E3FP-RDKit") produced no significant difference in fingerprint performance (Table 1). By design, this optimization and consequent performance analysis does not attempt to

quantify novelty of the predictions nor does it assess the false negative or untested-yet-true-positive rate of either method.

Having found that SEA-E3FP using RDKit-generated conformers outperformed SEA-ECFP4, we tested whether E3FP could still better enrich for known actives by using crystal structure conformers from the Protein Data Bank (PDB). Using SEA, we queried 32639 known ligands across 24 targets in ChEMBL20 that lacked crystal conformations against sets of 1446 unique target-bound ligands from the PDB. We generated E3FP fingerprints for ChEMBL20 using RDKit conformers as before while calculating the E3FP fingerprints for the PDB reference ligands on RDKit-generated (E3FP-RDKit) or crystal conformers (E3FP-PDB). While ECFP4's AUPRC of 0.5718 exceeded E3FP-RDKit's 0.5235 (SI, Figure S5A), E3FP-RDKit achieved a higher AUROC (0.8440 vs 0.8127) and AUC of the enrichment curve (AUEC) (0.8291 vs 0.7992) than ECFP4 (SI, Figure S5B,C). Interestingly, crystal conformers yielded poorer performance by all metrics, perhaps due to limitations of RDKit conformer generation. To test this, we repeated the same experiment using only the 1446 unique ligands from the PDB to populate test and train sets, with no ChEMBL test ligands, but the trend persisted (SI, Figure S5D−F).

We note that E3FP was optimized here for use with SEA, and SEA inherently operates on sets of fingerprints, such as those produced when fingerprinting a set of conformers. Most machine learning methods, however, operate on individual fingerprints. To determine how well E3FP could be integrated into this scenario, we repeated the entire ChEMBL-wide cross-validation with four common machine learning classifiers: Naive Bayes classifiers (NB), random forests (RF), support vector machines with a linear kernel (LinSVM), and artificial neural networks (NN). As these methods process each conformer independently, we computed the maximum score across all conformer-specific fingerprints for a given molecule and used that score for cross-validation. Operating on E3FP, the RF, NN, and LinvSVM classifiers matched or exceeded SEA PRC performance (SI, Figure S6), although only RF matched SEA's AUROC (SI, Figure S7). The same classifiers achieved higher AUPRCs using ECFP4 than E3FP, but at the cost of lower ROC performance for RF and LinSVM (SI, Figure S7). In general, the machine learning methods underperformed when using E3FP compared to ECFP4. When we instead took the bitwise mean of all conformer-specific E3FPs to produce one single summarizing "float" fingerprint per molecule, we observed an improvement across all machine learning methods except for LinSVM (by AUROC) and RF.

3D Fingerprints Encode Different Information than Their 2D Counterparts. 2D fingerprints such as ECFP4 may denote stereoatoms using special disambiguation flags or identifiers from marked stereochemistry (here termed "ECFP4-Chiral").[35] E3FP encodes stereochemistry more natively. Conceptually, all atoms within a spatial "neighborhood" and their relative orientations within that region of space are explicitly considered when constructing the fingerprint. To quantify how stereochemical information contributes to E3FP's improved AUPRC over that of ECFP4, we constructed three "2D-like" limited variants of E3FP, each of which omits some 3D information and is thus more analogous to ECFP. The first variant, which we term "E2FP," is a direct analogue of ECFP, in which only information from directly bound atoms are included in the identifier and stereochemistry is ignored. This variant produces similar ROC and PRC curves to that of ECFP4 (Figure 2C,D; SI, Figures S8−S9). A second variant, "E2FP-Stereo,"

includes information regarding the relative orientations of bound atoms. E2FP-Stereo achieves a performance between that of ECFP4 and E3FP, demonstrating that E3FP's approach for encoding stereochemical information is effective (Figure 2C,D). The third variant, "E3FP-NoStereo," includes only the information from bound and unbound atoms. E3FP-NoStereo performs slightly better than E3FP in both ROC and PRC analysis (Figure 2C,D), indicating that E3FP's enhanced performance over ECFP4 in PRC analysis is due not only to the relative orientations of atoms but also due to the inclusion of unbound atoms. All variants of E3FP with some form of 3D information outperformed both ECFP4 and ECFP4-Chiral (Figure 2C,D; SI, Figures S8−S9).

On average, the final E3FP parameters yield fingerprints with 35% more "on" bits than ECFP4, although if run for the same number of iterations, ECFP is denser. Thus, E3FP typically runs for more iterations (SI, Figure S4C,D). Folding E3FP down to 1024 bits results in an average loss of only 1.4 bits to collisions. The TCs for randomly chosen pairs of molecules by E3FP are generally lower (Figure 2A,B) than those for ECFP4, and there are fewer molecules with identical fingerprints by E3FP than by ECFP4. The final E3FP parameter set outperforms ECFP up to the same number of iterations (SI, Table S1; Figure 2C,D). Intriguingly, E3FP outperforms ECFP4 at this task on a per-target basis for a majority of targets (Figure 2F).

We assessed E3FP's performance relative to several other 3D molecular comparison methods. First, we used FastROCS to compute maximum ROCS shape (ROCS-shape) and shape plus color (ROCS-combo) TCs among all molecules in ChEMBL20, on the same set of conformers used for E3FP. This took six days using eight graphics processing units (GPUs), or approximately 74.7 central processing unit (CPU) years (SI, Table S3). We then performed 5-fold cross-validation to enrich for correct ligands (actives) by maximum pairwise TC. E3FP and ECFP4 achieved the highest areas under the enrichment curve (AUECs) of 0.9907 and 0.9918, whereas ROCS-shape achieved an AUEC of 0.9240, and ROCS-combo achieved an AUEC of 0.9703 (SI, Figure S11a). Correspondingly, we observed a weak correlation between individual E3FP and ROCS conformer-pair scores, particularly for ROCS-combo (SI, Figure S11B−E). Finally, we asked how these methods would correlate with root-mean-square deviation (RMSD) on optimally aligned conformer pairs as a separate baseline. To address this, we randomly sampled 1000 pairs, typically comparing one molecule's conformer to a conformer of another molecule, and found that none of the above methods was a good predictor of RMSD on maximum common substructure (MCS; SI, Figure S12A−D). However, we observed better correlations with RMSD when we recomputed these analyses, as well as the 3D pharmacophoric torsion fingerprint deviation (TFD),[29] using 10000 random same-molecule conformers instead (SI, Figure S12E−H).

Fourteen Molecular Pairs where 3D and 2D Fingerprints Disagree. To explore cases where E3FP and ECFP4 diverge, we computed E3FP versus ECFP4 pairwise similarity scores (Tanimoto coefficients; TCs) for all molecule pairs in ChEMBL20 (red markers in Figure 2A). We then manually inspected pairs from four regions of interest. Pairs representative of overall trends were selected, with preference toward pairs that had been assayed against the same target (SI, Table S4). The first region contains molecule pairs with TCs slightly above the SEA significance threshold for E3FP but below the threshold for ECFP4 (denoted by "x" markers). These predominantly comprise small compact molecules, with common atom types
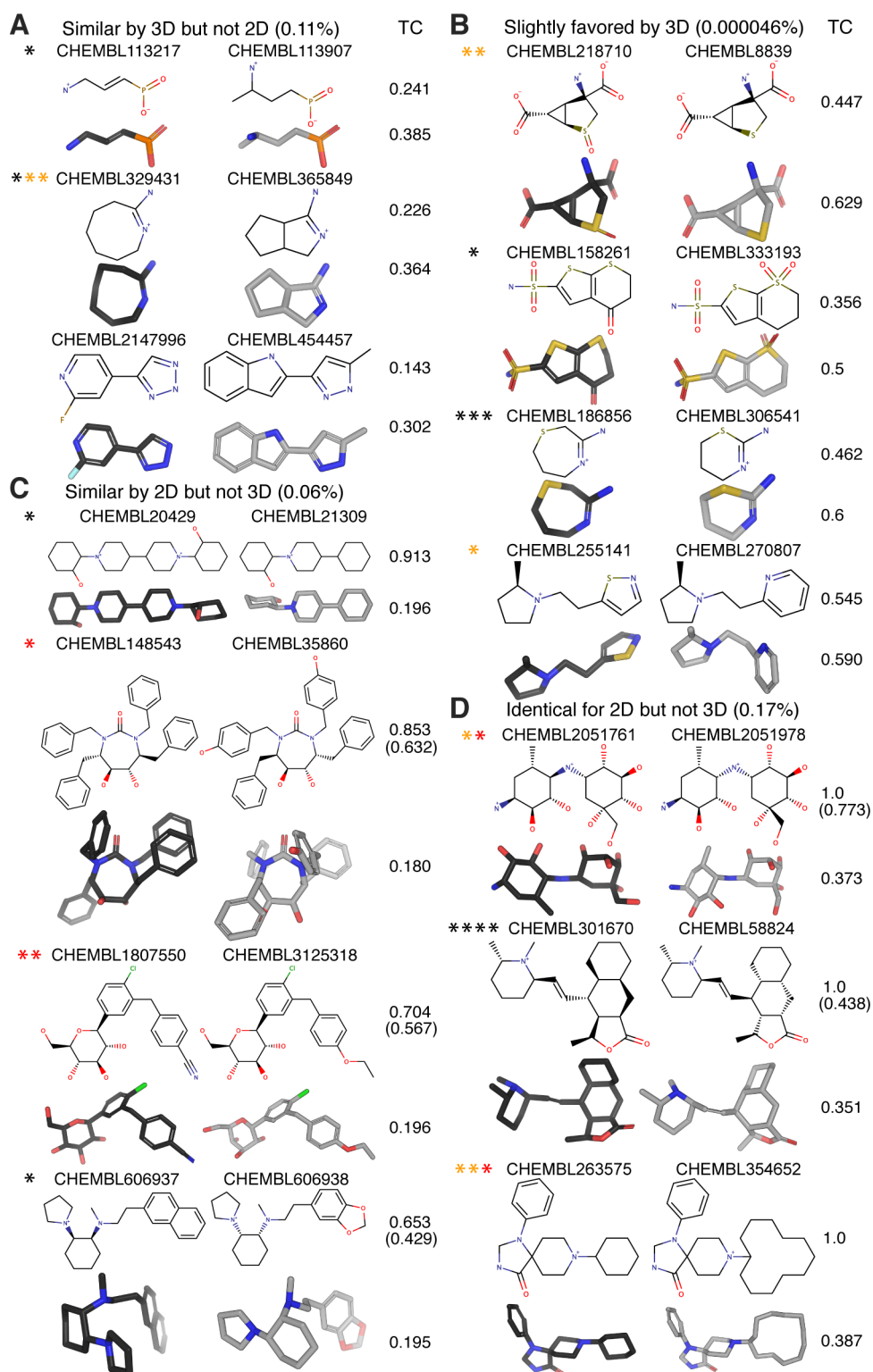
Figure 3. Examples of molecule pairs with high differences between E3FP and ECFP4 Tanimoto coefficients. Molecule pairs were manually selected from regions of interest, displayed as red markers in Figure 2A: (A) upper left, (B) upper right, (C) lower right, and (D) far right. Pair TCs for ECFP4 and E3FP are shown next to the corresponding 2D and 3D representations; the conformer pairs shown are those corresponding to the highest pairwise E3FP TC. Where pair TCs for ECFP4 with stereochemical information differ from standard ECFP4, they are included in parentheses. Each colored asterisk indicates a target for which existing affinity data for both molecules was found in the literature and is colored according to fold-difference in affinity: black for <10-fold, orange for 10−100-fold, and red for >100-fold. Further references for all compounds shown, including CHEMBL2147996[25] and CHEMBL454457,[25] may be found in SI, Table S4.

across multiple orders or substituents on rings (Figure 3A). Some of these molecules are already reported to interact with the same protein targets. For instance, CHEMBL113217[25] binds to

GABA-B receptor with an IC_{50} of 280 nM, while CHEMBL113907[25] binds GABA-B with a similar IC_{50} of 500 nM (Figure 3A).[49] In another example, CHEMBL329431[25]
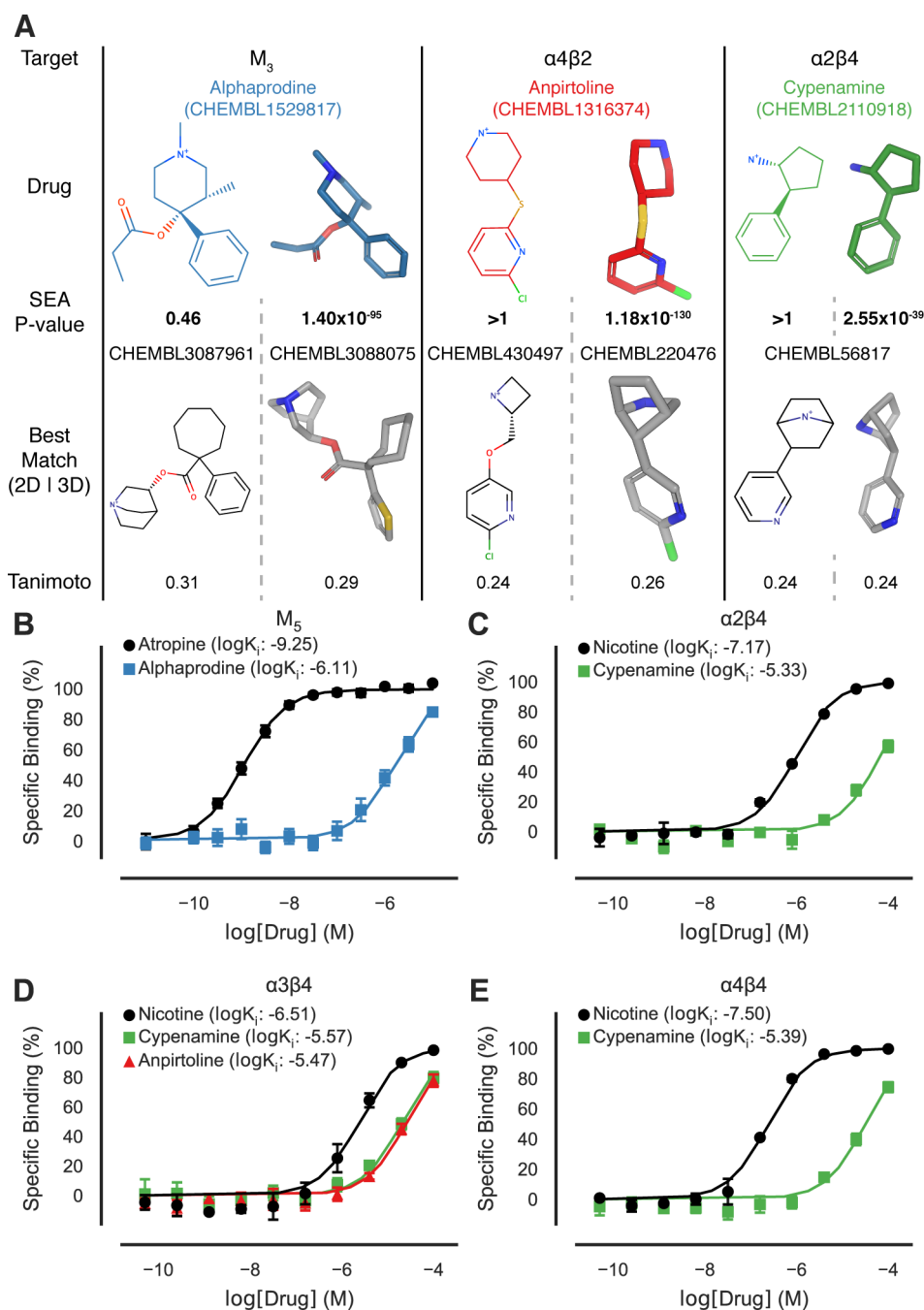
Figure 4. Experimental results of novel compound−target predictions. (A) SEA predictions that motivated the binding experiments, with 2D versus 3D SEA *p-value*s for each drug−target pair. Tanimoto coefficients score the similarity of 2D versus 3D structures for the searched drug against its most similar known ligand(s) of the target by ECFP4 (left) and E3FP (right). E3FP uses an early parameter set. Supporting Information, Table S5, shows recalculated SEA *p-value*s on the final E3FP parameter set used elsewhere. SEA *p-value* >1 denotes cases lacking TC above the SEA threshold (SI, Figure S13D−E), such that no *p-value* could be calculated. (B−E) Experimentally measured binding curves for tested drugs and reference binders (black) at protein targets (B) M_5, (C) $\alpha 2\beta 4$, (D) $\alpha 3\beta 4$, and (E) $\alpha 4\beta 4$. See SI, Table S8, for more details. All compounds shown, including CHEMBL3087961, CHEMBL3088075, CHEMBL430497, CHEMBL220476, and CHEMBL56817, are from ChEMBL20.[25]

binds to inducible, brain, and endothelial human nitric oxide synthases with IC_{50}s of 10.0, 10.1, and 59 μM, respectively,[50] while CHEMBL365849[25] binds to the same targets at 3.1 μM, 310 nM, and 4.7 μM.[51] The black asterisk alongside this pair marks similar affinities for the first target (within one log), and the orange asterisks affinities for the second two, each spanning two logs. Red asterisks mark targets whose affinities differ by more than two logs, but no such cases were found for this region.

The second region (red crosses in Figure 2A) contains molecule pairs with TCs considered significant both in 2D and in 3D but whose similarity was nonetheless greater by 3D (Figure 3B). For instance, the molecule pairs often differed by atom types in or substituents on a ring despite a high degree of similarity in 3D structures. In the case of CHEMBL158261[25] and CHEMBL333193,[25] the molecules bind to carbonic anhydrase II with near-identical affinities of 3.6 and 3.3 nM.[52] Interestingly, the 2D similarity of this pair is barely above the significance

threshold. In another example, the molecules CHEMBL186856[25] and CHEMBL306541[25] achieve markedly similar pharmacological profiles, as the first binds to the inducible, brain, and endothelial human nitric oxide synthases with IC_{50}s of 1.2, 2.8, and 10.5 μM,[53] whereas the second was reported at 2.9, 3.2, and 7.1 μM.[54] On the other hand, two other pairs somewhat differ in binding profile: while CHEMBL218710[25] binds to metabotropic glutamate receptors 2 and 3 with K_is of 508 and 447 nM, CHEMBL8839[25] binds to these targets more potently, at 40.6 and 4.7 nM.[55] Likewise, the binding profiles of CHEMBL255141[25] and and CHEMBL270807[25] to histamine H3 receptor differed by approximately an order of magnitude, with respective K_is of 17 and 200 nM.[56]

The third region (red squares in Figure 2A) contains molecule pairs significant in 2D but not in 3D (Figure 3C), and the fourth region (red diamonds in Figure 2A) contains pairs identical by 2D yet dissimilar in 3D (Figure 3D). These examples span several categories: First, the conformer generation protocol failed for some pairs of identical or near-identical molecules having many rotatable bonds because we generated an insufficient number of conformers to sample the conformer pair that would attain high 3D similarity between them (not shown). Second, in cases where the 2D molecules do not specify chirality, the specific force field used may favor different chiralities, producing artificially low 3D similarity. As an example, CHEMBL20429[25] and CHEMBL21309[25] (Figure 3C) have relatively similar affinities for vesicular acetylcholine transporter at 200 and 40 nM[57] despite their low 3D similarity. Third, some pairs consist of molecules primarily differentiated by the size of one or more substituent rings (Figure 3C,D). ECFP4 is incapable of differentiating rings with five or more identical atom types and only one substituent, while E3FP substructures may include larger portions of the rings. The role of ring size is revealed in the target affinity differences for one such pair: CHEMBL263575[25] binds to the κ opioid, μ opioid, and nociceptin receptors with K_is of 100, 158, and 25 nM, while CHEMBL354652[25] binds to the same receptors notably more potently at 2.9, 0.28, and 0.95 nM.[58] Fourth, many pairs consist of molecules primarily differentiated by the order of substituents around one or more chiral centers (Figure 3C,D). The molecules CHEMBL148543[25] and CHEMBL35860,[25] for example, bind to HIV type 1 protease with disparate K_is of 560[59] and 0.12 nM[60] despite their exceptionally high 2D similarity of 0.853 TC. Likewise, CHEMBL1807550[25] and CHEMBL3125318[25] have opposing specificities for the human sodium/glucose cotransporters 1 and 2; while the former has IC_{50}s of 10 nM and 10 μM for the targets,[61] the latter has IC_{50}s of 3.1 μM and 2.9 nM.[62] In another example, despite being identical by standard 2D fingerprints, the stereoisomers CHEMBL2051761[25] and CHEMBL2051978[25] bind to maltase–glucoamylase with IC_{50}s of 28 nM versus 1.5 μM, and to sucrase–isomaltase at 7.5 nM versus 5.3 μM.[63] The stereoisomers CHEMBL301670[25] and CHEMBL58824,[25] however, show a case where 3D dissimilarity is a less effective guide, as both molecules bind to the muscarinic acetylcholine receptors M_1–M_4 with generally similar respective IC_{50}s of 426.58 nM versus 851.14 nM, 95.5 nM versus 851.14 nM, 1.6 μM versus 794.33 nM, and 173.78 nM versus 794.33 nM.[64] Similarly, CHEMBL606937[25] and CHEMBL606938[25] have low similarity in 3D but bind to the σ opioid receptor with IC_{50}s of 37 and 34 nM.[65]

E3FP Predicts Correct New Drug Off-Targets That Are Not Apparent in 2D.
As E3FP enhanced SEA performance in

retrospective tests (Figure 2C,D), we hypothesized that this combination might identify novel interactions as yet overlooked with two-dimensional fingerprints. We therefore tested whether SEA with E3FP would make correct drug-to-target predictions that SEA with ECFP4 did not make. Using a preliminary choice of E3FP parameters (SI, Table S5), we generated fingerprints for all in-stock compounds in the ChEMBL20 subset of the ZINC15 (zinc15.docking.org) database with a molecular weight under 800 Da. As our reference library, we extracted a subset of ChEMBL20 comprising 309 targets readily available for testing by radioligand binding assay in the Psychoactive Drug Screening Program (PDSP)[66] database. The distribution of Tanimoto coefficients between these two molecule sets resembles that of pairwise molecules in ChEMBL20 (Figure 2; SI, Figure S13A,B). Histograms plotting representative drug pairwise similarities against the ligand sets of their predicted targets (SI, Figure S13C−E) demonstrate that almost all ECFP4 TC fall below the SEA TC cutoff for significance, while approximately half of E3FP's TCs exceed its SEA TC cutoff. Using SEA on this library, we identified all drug-to-target predictions with a *p-value* stronger than 1×10^{-25}. To focus on predictions specific to E3FP, we removed all predictions with a *p-value* stronger than 0.1 when counter-screened by SEA with ECFP4, resulting in 9331 novel predicted interactions. We selected eight predictions for testing by binding assay; of these, five were inconclusive and three bound to the predicted target subtype or to a close subtype of the same receptor (SI, Tables S5−S8). We address each of the latter in turn.

The E3FP SEA prediction that the psychostimulant and antidepressant[67−69] cypenamine (CHEMBL2110918), for which we could find no accepted targets in the literature despite its development in the 1940s, would bind to the human nicotinic acetylcholine receptor (nAchR) $\alpha2\beta4$ was borne out with a K_i of 4.65 μM (Figure 4C; SI, Table S8). Of note, this corresponds to a high ligand efficiency (LE) of 0.610 kcal/mol/heavy atom (see Experimental Section). An LE greater than 0.3 kcal/mol/heavy atom is generally considered a promising drug candidate.[70] As any prediction is only as specific as the reference ligand data from ChEMBL upon which it was based, we assayed cypenamine against multiple subtypes of nAchR. Cypenamine also bound to the nAchR subtypes $\alpha3\beta4$ and $\alpha4\beta4$ with K_i's of 2.69 and 4.11 μM (Figure 4D,E; SI, Table S8) and ligand efficiencies of 0.637 and 0.616 kcal/mol/heavy atom.

Anpirtoline (CHEMBL1316374) is an agonist of the 5-HT_{1B}, 5-HT_{1A}, and 5-HT_2 receptors and an antagonist of the 5-HT_3 receptor, with K_i's of 28, 150, 1490, and 30 nM, respectively.[71,72] However, we predicted it would bind to the nAchRs, of which it selectively bound to $\alpha3\beta4$ at a K_i of 3.41 μM and an LE of 0.536 kcal/mol/heavy atom (Figure 4D; SI, Table S8). In this case, the motivating SEA E3FP prediction was for the $\alpha4\beta2$ subtype of nAchR, for which the experiment was inconclusive, suggesting either that the ligand reference data from ChEMBL distinguishing these subtypes was insufficient or that the SEA E3FP method itself did not distinguish among them, and this is a point for further study.

Alphaprodine (CHEMBL1529817), an opioid analgesic used as a local anesthetic in pediatric dentistry,[73] bound to the muscarinic acetylcholine receptor (mAchR) M_5 with a K_i of 771 nM and an LE of 0.442 kcal/mol/heavy atom (Figure 4B; SI, Figure S14E). We found no agonist activity on M_5 by alphaprodine by Tango assay[74,75] (SI, Figure S15B), but we did find it to be an antagonist (SI, Figure S16). Intriguingly, alphaprodine also showed no significant affinity for any of the

muscarinic receptors M_1–M_4 up to 10 μM (SI, Figure S14A–D), indicating that it is an M_5-selective antagonist. Muscarinic M_5 selective small molecules are rare in the literature.[76] Whereas its M_5 selectivity would need to be considered in the context of its opioid activity (μ, κ, and δ opioid receptor affinities, however, are not publicly available), alphaprodine nonetheless may find utility as a M_5 chemical probe, given the paucity of subtype-selective muscarinic compounds. Interestingly, the E3FP SEA prediction leading us to the discovery of this activity was for the muscarinic M_3 receptor, to which alphaprodine ultimately did not bind and for which alphaprodine showed no agonist activity (SI, Figure S15A). This highlights not only the limitations of similarity-based methods such as SEA for the discovery of new subtype-selective compounds when none of that type are previously known but also the opportunity such methods provide to identify chemotypes and overall receptor families that merit further study nonetheless.

■ DISCUSSION AND CONCLUSIONS

Three results emerge from this study. First, we encode a simple three-dimensional molecular representation into a new type of chemical informatic fingerprint, which may be used to compare molecules in a manner analogous to that already used for two-dimensional molecular similarity. Second, the 3D fingerprints contain discriminating information that is naturally absent from 2D fingerprints, such as stereochemistry and relationships among atoms that are close in space but distant in their direct bond connectivity. Finally, as small molecules may adopt many structural conformations, we combine conformation-specific 3D fingerprints into sets to evaluate entire conformational ensembles at once. This may be of interest in cases where different conformations of a molecule are competent at diverse binding sites across the array of proteins for which that same molecule is, at various potencies, a ligand.

We devised a simple representation of three-dimensional molecular structures, an "extended 3D fingerprint" (E3FP), that is directly analogous to gold standard two-dimensional approaches such as the extended connectivity fingerprint (ECFP). As with two-dimensional fingerprints, this approach enables precalculation of fingerprints for all conformers of interest in an entire library of molecules once. Unlike conventional 3D approaches, similarity calculations in E3FP do not require an alignment step. Consequently, E3FP similarity calculations are substantially faster than standard 3D comparison approaches such as ROCS (SI, Table S3, Figure S10). Furthermore, E3FP fingerprints are formatted identically to ECFP and other 2D fingerprints. Thus, systems pharmacology approaches such as SEA,[4,5] naïve Bayes classifiers,[11] SVM,[14] and other established machine learning methods may readily incorporate E3FPs for molecular conformers without modification. While choices of E3FP's parameter space might be specifically optimized for the machine learning method in question, we have demonstrated that E3FP's highest-performing parameter choice for SEA (Figure 2C,D) produces fingerprints that likewise perform well for SVM, random forests, and neural networks (SI, Figures S6–S7).

To explore the role of 2D vs 3D features in the discriminatory power of molecular fingerprints, we progressively disabled capabilities specific to E3FP, such as stereochemistry encoding (termed "E3FP-NoStereo") and nonbonded atom relationships (termed "E2FP-Stereo"), eventually arriving at a stripped-down version of E3FP (termed "E2FP") that, much like ECFP, encodes only 2D information. We evaluated the consequences of removing these three-dimensional features on performance in retrospective machine learning tasks (e.g., Figure 2C–E, Table 1; SI, Figures S8–S9). We found that inclusion of nonbonded atoms was a more important contributor to performance than stereochemical information. Intriguingly, while progressively adding stereochemical information and inclusion of nonbonded atoms produces marked improvement over ECFP4, inclusion only of nonbonded atom information produces the highest performance fingerprint of all, perhaps because 3D orientations of larger substructures are implicitly encoded within shells purely by relative distances. This observation leads us to believe that a more balanced inclusion of stereochemical information and nonbonded atoms may produce an even higher performing fingerprint. Historically, 3D representations have typically underperformed 2D ones such as ECFP,[7] and this has always been the case with similarity ensemble approach (SEA) calculations in particular.[6] Here, however, we find that E3FP exceeds the performance of ECFP4 in its precision-recall curve (PRC) and matches that of ECFP4 in its receiver-operating characteristic curve (ROC) area under the curve (AUC) scores (Figure 2C–E, Table 1; SI, Figures S8–S9). While the ROC curve evaluates the general usefulness of the fingerprint for classification by comparing sensitivity and specificity, the precision-recall evaluates how useful the method is for real cases where most tested drug–target pairs are expected to have no affinity. The increased performance in PRC curves when using E3FP over ECFP4 therefore indicates an increased likelihood of predicting novel drug–target pairs that will be experimentally born out with no loss in predictive power.

E3FP's utility for this task became especially clear when we used it to predict novel drug to protein binding interactions. To do so, we examined only strong SEA predictions with E3FP (SEA-E3FP; *p-value* $\leq 1 \times 10^{-25}$) that could not be predicted using SEA with ECFP4 (SEA-ECFP; *p-value* $\geq$ 0.1). We considered this a challenging task because on-market drugs might be expected to have fewer unreported off-targets in general than a comparatively newer and less-studied research compound might. Furthermore, much of the prior work in chemical informatics guiding molecule design and target testing has been motivated by 2D approaches.[2,7,77] Accordingly, approximately half of the new predictions were inconclusive in this first prospective test of the method (SI, Tables S5 and S7). Nonetheless, many also succeeded with high ligand efficiencies (LEs), and these included unique selectivity profiles (Figure 4). In one example, SEA-E3FP successfully predicted that alphaprodine would also act as an antagonist of the M_5 muscarinic receptor, which to our knowledge is not only a new "off-target" activity for this drug but also constitutes a rare, subtype-selective M_5 antimuscarinic ligand.[76] The M_5 muscarinic receptor has roles in cocaine addiction,[78] morphine addiction,[79] and dilation of cerebral blood vessels, with potential implications for Alzheimer's disease.[80] Study of M_5 receptors has been hindered by a lack of selective ligands. Because of serious adverse reactions,[81] alphaprodine was withdrawn from the market in the United States in 1986 and is therefore unlikely to be applied as a therapeutic. However, alphaprodine might be explored not only as a chemical probe for studying M_5, but also as a reference for future therapeutic development.

Anpirtoline and cypenamine, likewise predicted and subsequently experimentally confirmed to bind previously unreported off-targets among the nicotinic receptors, exhibited exceptional LEs (0.536–0.637 kcal/mol/heavy atom), a commonly used metric of optimization potential. Recent patents

combining psychostimulants with low-dose antiepileptic agents for the treatment of attention deficit hyperactivity disorder (ADHD) incorporate cypenamine,[82,83] and nicotinic agents improve cognition and combat ADHD.[84] Given likewise the association of nicotinic acetylcholine receptor (nAchR) α4 gene polymorphisms with ADHD,[85] a combination of traditional psychostimulant activity with "non-stimulant" nAChR activity via α4 might improve anti-ADHD efficacy. Whereas cypenamine's micromolar binding concentration to nAchR is likely below the plasma concentrations it reaches at steady state, its exceptional LEs at nAchR may support further optimization of this pharmacology. As with cypenamine, anpirtoline may serve as a well-characterized starting point for further nAchR optimization, and secondarily, its serotonergic activity may serve as a guide to explore cypenamine's likely serotonergic activity. Anpirtoline's benign side effect profile, combined with the nAchR α3β4 subunit's role in nicotine addiction[86] and the lack of α3β4 specific drugs,[87] motivate further exploration.

We find that, whereas E3FP's performance matches or exceeds that of ECFP4 under multiple retrospective metrics, and whereas it leads to new off-target predictions complementing those of ECFP4 with SEA, there are cases where the more traditional 2D representation yields higher retrospective performance. It would be difficult to tease out the impact that 2D has of necessity made in guiding the design and testing of such molecules, and only time will tell whether ECFP4's higher performance in these cases is due to true pharmacology or historical bias. However, we currently find that ECFP4 outperforms E3FP on specific targets using SEA (Figure 2F) and in general when applying other machine learning methods (SI, Figures S6−S7). Similarly, ECFP4 performs well on highly flexible molecules, owing to the difficulty of a small conformer library representing the flexibility of these molecules. Conversely, E3FP's potential for discerning similar target binding profiles is best realized when comparing molecules with a high degree of conformational similarity on the one hand or on the other one or more chiral centers. As is evident from their respective PRC plots, E3FP typically discriminates SEA predictions more than ECFP4 does, thereby achieving a better precision-recall ratio at the initial cost of some sensitivity (Figure 2C). However, this also allows E3FP to consider more distant molecular similarity relationships while maintaining greater discriminatory power than ECFP4 does at this range. It would be interesting to explore whether some of these more distant relationships might also be regions of pharmacological novelty.

One longtime advantage of 2D molecular representations has been their ability to implicitly sidestep the question of conformation. Whereas heroic effort has gone into solving the crystallographic conformations of hundreds of thousands of small molecules,[88,89] the binding-competent 3D conformations for millions of research[25] and purchasable[32] small molecules are not known. Furthermore, polypharmacology exacerbates this problem, wherein a single small molecule can bind many protein partners, as it is not always the case that the molecule in question will adopt the same conformation for each binding site.[2] Powerful methods to enumerate and energetically score potential conformations exist,[90−92] but it falls to the researcher to prioritize which of these conformers may be most relevant for a given protein or question. Treating the top five, ten, or more most energetically favorable conformers as a single set, however, may be an alternate solution to this problem. We originally developed SEA so as to compare entire sets of molecular fingerprints against each other,[4] so it seemed natural to use it in a conformational-set-

wise manner here. Furthermore, because SEA capitalizes on nearest-neighbor similarities among ligands across sets of molecules, we expected that it might analogously benefit from nearest-neighbor similarities in conformational space on a protein-by-protein basis. This may indeed be the case, although we have not attempted to deconvolve E3FP's performance in a way that would answer whether different E3FPs, and hence different conformations, of the same molecule most account for its predicted binding to different protein targets.

The E3FP approach is not without its limitations. E3FP fingerprints operate on a pregenerated library of molecular conformers. The presence of multiple conformers and therefore multiple fingerprints for a single molecule hampers machine learning performance in naive implementations (SI, Figures S6−S7), as flexible molecules dominate the training and testing data. We anticipate higher numbers of accepted conformers to only exacerbate the problem. The full conformational diversity of large, flexible molecules pose a substantial representational challenge as well (Figure 3C,D). As E3FP depends upon conformer generation, a generator that consistently imposes specific stereochemistry on a center lacking chiral information may produce artificially low or high 3D similarity (Figure 3C). Furthermore, the core intuition of E3FP hinges on the assumption that most binding sites will have differing affinities for molecules with diverging stereochemical orientations, such as stereoisomers. Because of site flexibility, this is not always the case (Figure 3C,D).

Despite these caveats, we hope that this simple, rapid, and conformer-specific extended three-dimensional fingerprint (E3FP) will be immediately useful to the broader community. To this end, we have designed E3FP to integrate directly into the most commonly used protein target prediction methods without modification. An open-source repository implementing these fingerprints and the code to generate the conformers used in this work is available at https://github.com/keiserlab/e3fp/tree/1.1.

EXPERIMENTAL SECTION

Generating Conformer Libraries. To maximize reproducibility, we generated conformers following a previously published protocol[38] using RDKit.[93] For each molecule, the number of rotatable bonds determined the target number of conformers, N, such that $N = 50$ for molecules with less than 8 rotatable bonds, $N = 200$ for molecules with 8−12 rotatable bonds, and $N = 300$ for molecules with over 12 rotatable bonds. We generated a size $2N$ pool of potential conformers.

After minimizing conformers with the Universal Force Field[92] in RDKit, we sorted them by predicted energy. The lowest energy conformer became the seed for the set of accepted conformers. We considered each candidate conformer in sorted order, calculated its root-mean-square deviation (RMSD) to the closest accepted conformer, and added the candidate to the accepted set if its RMSD was beyond a predefined distance cutoff R. Optionally, we also enforced a maximum energy difference E between the lowest and highest energy accepted conformers. After having considered all $2N$ conformers, or having accepted N conformers, the process terminated, yielding a final set of conformers for that molecule.

We tuned this protocol using three adjustable parameters: (1) the minimum RMSD between any two accepted conformers, (2) the maximum computed energy difference between the lowest energy and highest energy accepted conformers, and (3) the number of lowest energy conformers to be accepted (fingerprinted). We generated two different conformer libraries by this protocol. In the first (rms0.5), we used a RMSD cutoff $R = 0.5$, with no maximum energy difference E. In the second (rms1_e20), we chose a RMSD cutoff $R = 1.0$, with a maximum energy difference of 20 kcal/mol.

Enumerating Protonation States. Where specified, we generated dominant tautomers at pH 7.4 from input SMILES using the CXCALC

program distributed with ChemAxon's Calculator Plugins.[94] We kept the first two protonation states with at least 20% predicted occupancy. Where no states garnered at least 20% of the molecules, or where protonation failed, we kept the input SMILES unchanged. Conformer generation for each tautomer proceeded independently and in parallel.

ECFP Fingerprinting. To approximate ECFP fingerprints, we employed the Morgan fingerprint from RDKit using default settings and an appropriate radius. ECFP4 fingerprints, for example, used a Morgan fingerprint of radius 2. Where ECFP with stereochemical information is specified, the same fingerprinting approach was used with chirality information incorporated into the fingerprint. An ECFP fingerprint is a bitvector, where a specific bit indicates the presence of a 2D molecular substructure at a given circular radius.

E3FP Fingerprinting. Given a specific conformer for a molecule, E3FP generates a 3D fingerprint, parametrized by a shell radius multiplier r and a maximum number of iterations (or level) L, analogous to half of the diameter in ECFP. E3FP explicitly encodes stereochemistry. As with ECFP, an E3FP fingerprint is by default a bitvector, where a specific bit indicates the presence of a 3D molecular substructure.

Generating Initial Identifiers. Like ECFP, E3FP generation is an iterative process and can be terminated at any iteration or upon convergence. At iteration 0, E3FP generation begins by determining initial identifiers for each atom based on seven atomic properties, identical to the invariants described in[35] the number of heavy atom immediate neighbors, the valence minus the number of neighboring hydrogens, the atomic number, the atomic mass, the atomic charge, the number of bound hydrogens, and whether the atom is in a ring. For each atom, the array of these values are hashed into a 32-bit integer, the atom identifier at iteration 0. While the hashing function is a matter of choice, so long as it is uniform and random, this implementation used MurmurHash3.[95]

Generating Atom Identifiers at Each Iteration. At each iteration i where $i > 0$, we considered each atom independently. Given a center atom, the set of all atoms within a spherical shell of radius $i \cdot r$ centered on the atom defines its immediate neighborhood, where the parameter r is the shell radius multiplier (Figure 1A). We initialize an array of integer tuples with a number pair consisting of the iteration number i and the identifier of the central atom from the previous iteration.

For each noncentral atom within the shell, we added to the array an integer 2-tuple consisting of a connectivity identifier and the atom's identifier from the previous iteration. The connectivity identifiers were enumerated as an expanded form of those used for ECFP: the bond order for bond orders of 1−3, 4 for aromatic bonds, and 0 for neighbors not bound to the central atom. To avoid dependence on the order in which atom tuples were added to the array, we sorted the positions of all but the first tuple in ascending order. The 3-tuples were then formed through the addition of a stereochemical identifier, followed by resorting. This process is described in detail below.

We then flatten the completed array into a one-dimensional integer array. We hash this 1D array into a single new 32-bit identifier for the atom and add it to an identifier list for the iteration after optional filtering described below.

Adding Stereochemical Identifiers. We generated stereochemical identifiers by defining unique axes from the sorted integer 2-tuples from the previous step combined with spatial information. First, we determined the vectors from the center atom to each atom within the shell. Then, we selected the first unique atom by atom identifier from the previous iteration, if possible, and set the vector from the central atom to it as the y-axis. Where this is not possible, we set the y-axis to the average unit vector of all neighbors. Using the angles between each unit vector and the y-axis, the atom closest to 90° from the y-axis with a unique atom identifier from the previous iteration defines the vector of the x-axis (Figure 1A).

We then assigned integer stereochemical identifiers s. Atoms in the $y > 0$ and $y < 0$ hemispheres have positive and negative identifiers, respectively. $s = \pm1$ was assigned to atoms whose unit vectors fall within 5° of the y-axis. We divided the remaining surface of the unit sphere into eight octants, four per hemisphere. The x-axis falls in the middle of the $s = \pm2$ octants, and identifiers $\pm3-5$ denote remaining octants radially

around the y-axis (Figure 1A). If unique y- and x-axes assignment fails, all stereochemical identifiers are set to 0.

Combining the connectivity indicator and atom identifier with the stereochemical identifier forms a 3-tuple for each atom, which, when hashed, produces an atom identifier dependent orientation of atoms within the shell.

Removing Duplicate Substructures. Each shell has a corresponding *substructure* defined as the set of atoms whose information is contained within the atoms in a shell. It includes all atoms within the shell on the current iteration as well as the atoms within their substructures in the previous iteration. Two shells have the same substructure when these atom sets are identical, even when the shell atoms are not. As duplicate substructures provide little new information, we filtered them by only adding the identifiers to that iteration's list that correspond to new substructures or, if two new identifiers correspond to the same substructure, the lowest identifier.

Representing the Fingerprint. After E3FP runs for a specified number of iterations, the result is an array of 32-bit identifiers. We interpreted these as the only "on" bits in a 2^{32} length sparse bitvector, and they correspond to 3D substructures. As with ECFP, we "folded" this bitvector to a much smaller length such as 1024 by successively splitting it in half and conducting bitwise OR operations on the halves. The sparseness of the bitvector results in a relatively low collision rate upon folding.

Variants of E3FP. For comparisons against ECFP, we disabled specific features of the E3FP fingerprinting process to determine the contribution of that feature to E3FP's overall performance. Unlike ECFP, full E3FP considers neighboring atoms that are not bound to the central atom. Disabling this feature produces a similar fingerprint to ECFP, termed "E2FP-Stereo", because it still contains stereochemical identifiers. Additionally, disabling stereochemical identifiers produces a very similar fingerprint to default ECFP, which we term "E2FP". Conversely, if we disabled only the addition of stereochemical identifiers while still considering unbound neighbors, we produced the "E3FP-NoStereo" fingerprint.

Fingerprint Set Comparison with SEA. The similarity ensemble approach (SEA) is a method for searching one set of bitvector fingerprints against another set.[4] SEA outputs the maximum Tanimoto coefficient (TC) between any two fingerprint sets and a *p-value* indicating overall similarity between the sets. SEA first computes all pairwise TCs between the two fingerprint sets. The sum of all TCs above a preset pairwise TC threshold T defines a *raw score*. For a given fingerprint, SEA calculates a background distribution of raw scores empirically.[4] This yields an observed *z-score* distribution, which at suitable values of T follows an extreme value distribution (EVD). For values of T ranging from 0 to 1, comparing goodness of fit (*chi-square*) to an EVD vs a normal distribution determines an optimal range of T, where the empirical *z-score* distribution favors an EVD over a normal distribution. In this EVD regime we may convert a *z-score* to a *p-value* for any given set−set comparison.

k-Fold Cross-Validation with SEA. We performed k-fold cross-validation on a target basis by dividing the ligands of at least 10 μM affinity to each target into k sets per target. For a given fold, k-1 ligand sets and their target labels together formed the training data. The remaining ligand sets and their target labels formed the test data set. Because of the high number of negative examples in the test set, this set was reduced by ~25% by removing all negative target−molecule pairs that were not positive to any target in the test set. Conformers of the same ligand did not span the train vs test set divide for a target. For each fold, conformer fingerprint sets for molecules specific to the test set were searched against the union of all training conformer fingerprints for that target, yielding a molecule-to-target SEA *p-value*. From the −log *p-value*s for all test-molecule-to-potential-target tuples, we constructed a receiver operating characteristic (ROC) curve for each target, and calculated its area under the curve (AUC). We likewise calculated the AUC for the precision-recall curve (PRC) at each target. For a given fold, we constructed an ROC curve and a PRC curve using the −log *p-value*s and true hit/false hit labels for all individual target test sets, which we then used to compute a fold AUROC and AUPRC. We then computed an average AUROC and AUPRC across all k folds. The objective function

AUC$_{SUM}$ consisted of the sum of the average AUROC and AUPRC. For some analyses, we additionally computed the enrichment curve (EC), also known as cumulative recall curve, which reports the fraction of actives recovered (sensitivity) as a function of percent of database screened.[96]

Optimizing Parameters with Spearmint. E3FP fingerprints have the following tunable parameters: stereochemical mode (on/off), nonbound atoms excluded, shell radius multiplier, iteration number, and folding level. Additional tunable parameters for the process of conformer generation itself are the minimum RMSD between conformers, the maximum energy difference between conformers, and how many of the first conformers to use for searching. This parameter space forms an eight-dimensional hypercube. Of the eight dimensions possible, we employed the Bayesian optimization program Spearmint[48] to explore four: shell radius multiplier, iteration number, number of first conformers, and two combinations of values for the RMSD cutoff and maximum energy difference between conformers. We evaluated the parameter sets by an objective function summing ROC and PRC AUCs (AUC$_{SUM}$), and Spearmint proposed future parameter combinations. The objective function evaluated k-fold cross-validation with the similarity ensemble approach (SEA) as described in the following section.

For the first stage, the data set consisted of 10000 ligands randomly chosen from ChEMBL17, the subset of targets that bound to at least 50 of these ligands at 10 μM or better, and the objective function used was the AUPRC. Spearmint explored values of the shell radius multiplier between 0.1 and 4.0 Å, the number of lowest energy conformers ranging from 1 to all, and maximum iteration number of 5. Additionally, two independent conformer libraries were explored: rms0.5 and rms1_e20 (see above). Consequently, 343 unique parameter sets were explored. We found that the best parameter sets used less than 35 of the lowest energy conformers, a shell radius multiplier between 1.3 and 2.8 Å, and 2−5 iterations. The conformer library used did not have an apparent effect on performance (data not shown).

For the second stage, we ran two independent Spearmint trajectories with a larger data set consisting of 100000 ligands randomly chosen from ChEMBL20, the subset of targets that bound to at least 50 of these ligands at 10 μM or better, and the AUC$_{SUM}$ objective function. We employed the CXCALC program[94] to determine the two dominant protonation states for each molecule at physiological pH, and then conformers were generated using an RMSD cutoff of 0.5. The number of fingerprinting iterations used in both trajectories was optimized from 2 to 5, but the two trajectories explored different subsets of the remaining optimal parameter ranges identified during the first stage: the first explored shell radius multipliers between 1.3 and 2.8 Å with number of conformers bounded at 35, while the second explored shell radius multipliers between 1.7 and 2.8 Å with number of conformers bounded at 20. Spearmint tested 100 parameter combinations in each trajectory.

During optimization, we observed that the simple heuristic used by SEA to automatically select the TC threshold for significance resulted in folds with high TC cutoffs having very high AUPRCs but low AUROCs due to low recall, while folds with low TC cutoffs had lower AUPRCs but very high AUROCs (SI, Figure S3). Several folds in the latter region outperformed ECFP4 in both AUPRC and AUROC (SI, Figure S3c). We therefore selected the best parameter set as that which produced the highest AUC$_{SUM}$ while simultaneously outperforming ECFP4 in both metrics. For all future comparisons, the TC cutoff that produced the best fold results was applied to all folds during cross-validation.

***k*-Fold Cross-Validation with Other Classifiers.** We performed k-fold cross-validation using alternative classifiers in the same manner as for SEA, with the following differences. We trained individual classifiers on a target by target basis. In the training and test data, we naively treated each conformer fingerprint as a distinct molecular fingerprint, such that the conformer fingerprints did not form a coherent set. After evaluating the target classifier on each fingerprint for a molecule, we set the molecule score to be the maximum score of all of its conformer fingerprints.

For the naïve Bayes (NB), random forest (RF), and support vector machine with a linear kernel (LinSVM) classifiers, we used Scikit-learn version 0.18.1 (https://github.com/scikit-learn/scikit-learn/tree/0.18.

1). We used default initialization parameters, except where otherwise specified. For the RF classifier, we used 100 trees with a maximum depth of 25. We weighted classes (positive and negative target/molecule pairs) to account for class imbalance. For LinSVM kernel, we applied an l1 norm penalty and balanced class weights as for RF.

We implemented artificial neural network (NN) classifiers with nolearn version 0.6.0 (https://github.com/dnouri/nolearn/tree/0.6.0). We trained networks independently for each target using 1024-bit input representations from either E3FP or ECFP4. The NN architecture comprised three layers: an input layer, a single hidden layer with 512 nodes, and an output layer. We used dropout[97] as a regularizer on the input and hidden layers at rates of 10% and 25%, respectively. The hidden layer activation function was Leaky Rectified Linear[98] with default leakiness of 0.01. The prediction layer used softmax non-linearities. We trained networks trained for 1000 epochs with early stopping to avoid overfitting by monitoring the previous 75 epochs for lack of change in the loss function. The final softmax layer contained two tasks (classes), one corresponding to binding and the other corresponding to the absence of binding. This softmax layer produced a vector corresponding to the probability of a given molecule being a binder or nonbinder given the neural network model. We calculated training error using a categorical cross entropy loss.

Enriching for Actives Using PDB Ligands. To assess the impact of crystal conformers on E3FP's performance, we used target/ligand pairs annotated in scPDB v. 2013.[99] We filtered it to those 24 targets that could be mapped to ChEMBL20 and had at least 25 ligands in crystal conformations. The set of 1446 unique PDB ligands was the union of all ligands annotated to at least one of these targets. The query data set consisted of 32639 unique ligands from ChEMBL20 annotated to bind to one of the PDB targets, after removing all compounds found in the PDB data set. For ChEMBL20 ligands, we generated ECFP4 fingerprints and E3FP fingerprints using the conformer generation protocol described above (E3FP-RDKit). For PDB compounds, we generated the same fingerprints as well as an additional set of E3FP fingerprints using the crystal conformer (E3FP-PDB). Using each of the above representations, we queried ChEMBL20 compounds against PDB targets in a set-by-set validation using SEA and assessed performance by ROC, PRC, and EC curves. Additionally, we performed a separate 5-fold cross-validation on PDB-only ligands using SEA, where all train and test ligands were derived solely from the PDB set.

Comparing E3FP to Other 3D Methods. To compare performance of E3FP with other 3D methods, we computed pairwise ROCS shape and combo (shape + color) TCs between all molecule pairs in our ChEMBL20 data set using FastROCS (OpenEye Toolkits v2017.Jan) on GeForce 1080 GTX Founders Edition GPUs. We then performed enrichment analysis as described in "Enriching for Actives using PDB Ligands" on ChEMBL20 molecules by 5-fold cross-validation, evaluating comparative performance of ECFP4, E3FP, and ROCS by AUEC. To compare pairwise similarity scores from each method against RMSD, we computed ECFP4 TC, E3FP Max TC, ROCS-shape TC, and ROCS-combo TC for all pairs of 10000 random molecules. RMSDs were computed on the MCS between the two conformers, as determined by RDKit. Likewise, we computed each of the above 3D similarities on 10000 random same-molecule conformer pairs, in addition to the TFD pharmacophoric comparison implemented in RDKit.

Predicting Novel Compound-Target Binding Pairs. To identify novel compound-target pairs predicted by E3FP but not by ECFP4, we built a subset of 309 proteins/complex mammalian targets (106 human) for which the National Institute of Mental Health Psychoactive Drug Screening Program (NIMH PDSP)[66] had established binding assays. We selected all compounds listed as in-stock in ZINC15,[32] downloaded on 2015-09-24. We fingerprinted all ligands in ChEMBL20[25] with affinity <10 μM to the PDSP targets using the RDKit Morgan algorithm (an ECFP implementation) as well as by a preliminary version of E3FP (SI, Table S5). We likewise fingerprinted the ZINC15 compounds using both ECFP4 and E3FP. We queried the search compounds using SEA against a discrete sets of ligands from <10 nM affinity (strong binders) to <10 μM affinity (weak binders) to each target, in log-order bins, using both ECFP4 and E3FP independently. We filtered the resulting

predictions down to those with a strong SEA-E3FP *p-value* ($<1 \times 10^{-25}$) and $\leq$10 nM affinity to the target, where the SEA-ECFP *p-value* exceeded 0.1 (i.e., there was no significant SEA-ECFP prediction) in the same log-order affinity bin. From this set of compound−target pairs, we manually selected eight for experimental testing.

Experimental Assays of Compound-Target Binding Pairs. All active compounds were reported ≥95% pure by their vendor (SI, Table S6). Alphaprodine's purity was verified by NMR (SI, Figure S17) and LC-MS (SI, Figure S18). Anpirtoline was confirmed >99% pure by HPLC (SI, Table S6). All tested compounds were checked for promiscuous binding by binding assays against a large family of related targets (SI, Table S7).

Radioligand binding and functional assays were performed as previously described.[74,100,101] Detailed experimental protocols and curve fitting procedures are available on the NIMH PDSP Web site at: https://pdspdb.unc.edu/pdspWeb/content/PDSP%20Protocols%20II%202013-03-28.pdf. Ligand efficiencies were calculated using the expression

$$\text{LE} = -RT(\ln K_i)/N_{\text{heavy}} \approx -1.373\log_{10} K_i/N_{\text{heavy}}$$

where R is the ideal gas constant, T is the experimental temperature in Kelvin, and N_{heavy} is the number of heavy atoms in the molecule.[102] The ligand efficiency is expressed in units of kcal/mol/heavy atom.

Source Code. Code for generating E3FP fingerprints is available at https://github.com/keiserlab/e3fp/tree/1.1 under the GNU Lesser General Public License version 3.0 (LGPLv3) license. All code necessary to reproduce this work is available at https://github.com/keiserlab/e3fp-paper/tree/1.1 under the GNU LGPLv3 license.

ASSOCIATED CONTENT

ⓢ Supporting Information

The Supporting Information is available free of charge on the ACS Publications website at DOI: 10.1021/acs.jmedchem.7b00696.

Supporting figures and tables include an enlarged Figure 1C, parameter optimization and cross-validation results, additional comparisons to other fingerprints, references for highlighted molecule pairs in Figure 3, descriptions of compounds used in experiments, all experimental results (PDF)

Molecular formula strings (CSV)

AUTHOR INFORMATION

Corresponding Author

*Phone: 415-886-7651. E-mail: keiser@keiserlab.org.

ORCID ⓞ

Michael J. Keiser: 0000-0002-1240-2192

Notes

The authors declare no competing financial interest.

ACKNOWLEDGMENTS

ABBREVIATIONS USED

ADHD, attention deficit hyperactivity disorder; AUC, area under the curve; AUEC, area under the enrichment curve; AUPRC, area under the precision-recall curve; AUROC, area under the receiver operating characteristic curve; CPU, central processing unit; DNN, deep neural network; E2FP, E3FP with 3D features disabled; E3FP, extended three-dimensional fingerprint; EC, enrichment curve; ECFP, extended connectivity fingerprint; EVD, extreme value distribution; FEPOPS, feature point pharmacophores; GPU, graphics processing unit; LE, ligand efficiency; LinSVM, support vector machine with a linear kernel; mAchR, muscarinic acetylcholine receptor; MCS, maximum common substructure; NB, naive bayes classifier; nAchR, nicotinic acetylcholine receptor; NN, artificial neural network; OCEAN, optimized cross reactivity estimation; PDB, Protein Data Bank; PRC, precision-recall curve; PDSP, psychoactive drug screening program; RF, random forest; RMSD, root-mean-square deviation; ROC, receiver operating characteristic curve; ROCS, rapid overlay of chemical structures; SEA, similarity ensemble approach; SVM, support vector machine; TC, Tanimoto coefficient; TFD, torsion fingerprint deviation; ZINC, ZINC is not commercial

REFERENCES

(1) Matter, H. Selecting Optimally Diverse Compounds from Structure Databases: A Validation Study of Two-Dimensional and Three-Dimensional Molecular Descriptors. *J. Med. Chem.* **1997**, *40*, 1219−1229.

(2) Nicholls, A.; McGaughey, G. B.; Sheridan, R. P.; Good, A. C.; Warren, G.; Mathieu, M.; Muchmore, S. W.; Brown, S. P.; Grant, J. A.; Haigh, J. A.; Nevins, N.; Jain, A. N.; Kelley, B. Molecular Shape and Medicinal Chemistry: A Perspective. *J. Med. Chem.* **2010**, *53*, 3862−3886.

(3) Sheridan, R. P.; Kearsley, S. K. Why Do We Need so Many Chemical Similarity Search Methods? *Drug Discovery Today* **2002**, *7*, 903−911.

(4) Keiser, M. J.; Roth, B. L.; Armbruster, B. N.; Ernsberger, P.; Irwin, J. J.; Shoichet, B. K. Relating Protein Pharmacology by Ligand Chemistry. *Nat. Biotechnol.* **2007**, *25*, 197−206.

(5) Keiser, M. J.; Setola, V.; Irwin, J. J.; Laggner, C.; Abbas, A. I.; Hufeisen, S. J.; Jensen, N. H.; Kuijer, M. B.; Matos, R. C.; Tran, T. B.; Whaley, R.; Glennon, R. A.; Hert, J.; Thomas, K. L. H.; Edwards, D. D.; Shoichet, B. K.; Roth, B. L. Predicting New Molecular Targets for Known Drugs. *Nature* **2009**, *462*, 175−181.

(6) Hert, J.; Keiser, M. J.; Irwin, J. J.; Oprea, T. I.; Shoichet, B. K. Quantifying the Relationships among Drug Classes. *J. Chem. Inf. Model.* **2008**, *48*, 755−765.

(7) Maggiora, G.; Vogt, M.; Stumpfe, D.; Bajorath, J. Molecular Similarity in Medicinal Chemistry. *J. Med. Chem.* **2014**, *57*, 3186−3204.

(8) Keiser, M. J.; Irwin, J. J.; Shoichet, B. K. The Chemical Basis of Pharmacology. *Biochemistry* **2010**, *49*, 10267−10276.

(9) Chen, B.; Harrison, R. F.; Papadatos, G.; Willett, P.; Wood, D. J.; Lewell, X. Q.; Greenidge, P.; Stiefl, N. Evaluation of Machine-Learning Methods for Ligand-Based Virtual Screening. *J. Comput.-Aided Mol. Des.* **2007**, *21*, 53−62.

(10) Bender, A.; Mussa, H. Y.; Glen, R. C.; Reiling, S. Molecular Similarity Searching Using Atom Environments, Information-Based Feature Selection, and a Naïve Bayesian Classifier. *J. Chem. Inf. Comput. Sci.* **2004**, *44*, 170−178.

(11) Zhang, H. The Optimality of Naive Bayes. In *Proceedings of the Seventeenth International Florida Artificial Intelligence Research Society Conference, Miami Beach, FL, May 12−14, 2014*; 2004.

(12) Breiman, L. Random Forests. *Mach. Learn.* **2001**, *45*, 5−32.

(13) Svetnik, V.; Liaw, A.; Tong, C.; Culberson, J. C.; Sheridan, R. P.; Feuston, B. P. Random Forest: A Classification and Regression Tool for Compound Classification and QSAR Modeling. *J. Chem. Inf. Comput. Sci.* **2003**, *43*, 1947−1958.

(14) Cortes, C.; Vapnik, V. Support-Vector Networks. *Mach. Learn.* **1995**, *20*, 273−297.

(15) Franke, L.; Byvatov, E.; Werz, O.; Steinhilber, D.; Schneider, P.; Schneider, G. Extraction and Visualization of Potential Pharmacophore Points Using Support Vector Machines: Application to Ligand-Based Virtual Screening for COX-2 Inhibitors. *J. Med. Chem.* **2005**, *48*, 6997−7004.

(16) Ramsundar, B.; Kearnes, S.; Riley, P.; Webster, D.; Konerding, D.; Pande, V. Massively Multitask Networks for Drug Discovery. *arXiv: stat/1502.02072. arXiv.org e-Print archive*, 2015; https://arxiv.org/abs/1502.02072 (accessed April 14, 2015).

(17) Kearnes, S.; McCloskey, K.; Berndl, M.; Pande, V.; Riley, P. Molecular Graph Convolutions: Moving beyond Fingerprints. *J. Comput.-Aided Mol. Des.* **2016**, *30*, 595−608.

(18) Baskin, I. I.; Winkler, D.; Tetko, I. V. A Renaissance of Neural Networks in Drug Discovery. *Expert Opin. Drug Discovery* **2016**, *11*, 785−795.

(19) Unterthiner, T.; Mayr, A.; Klambauer, G.; Steijaert, M.; Wegner, J. K.; Ceulemans, H.; Hochreiter, S. Deep Learning as an Opportunity in Virtual Screening. *Neural Information Processing Systems Conference Deep Learning and Representation Learning Workshop, Montréal, Canada, December 8−13, 2014*; 2014.

(20) Dahl, G. E.; Jaitly, N.; Salakhutdinov, R. Multi-task Neural Networks for QSAR Predictions. *arXiv: stat/1406.1231. arXiv.org e-Print archive*, 2015; https://arxiv.org/abs/1406.1231 (accessed Jul 1, 2015).

(21) Czodrowski, P.; Bolick, W.-G. OCEAN: Optimized Cross REActivity EstimatioN. *J. Chem. Inf. Model.* **2016**, *56*, 2013−2023.

(22) Hawkins, P. C. D.; Skillman, A. G.; Nicholls, A. Comparison of Shape-Matching and Docking as Virtual Screening Tools. *J. Med. Chem.* **2007**, *50*, 74−82.

(23) Rush, T. S.; Grant, J. A.; Mosyak, L.; Nicholls, A. A Shape-Based 3-D Scaffold Hopping Method and Its Application to a Bacterial Protein-Protein Interaction. *J. Med. Chem.* **2005**, *48*, 1489−1495.

(24) Haque, I. S.; Pande, V. S. SCISSORS: A Linear-Algebraical Technique to Rapidly Approximate Chemical Similarities. *J. Chem. Inf. Model.* **2010**, *50*, 1075−1088.

(25) Bento, A. P.; Gaulton, A.; Hersey, A.; Bellis, L. J.; Chambers, J.; Davies, M.; Krüger, F. A.; Light, Y.; Mak, L.; McGlinchey, S.; Nowotka, M.; Papadatos, G.; Santos, R.; Overington, J. P. The ChEMBL Bioactivity Database: An Update. *Nucleic Acids Res.* **2014**, *42*, D1083−1090.

(26) Sun, J.; Jeliazkova, N.; Chupakhin, V.; Golib-Dzib, J.-F.; Engkvist, O.; Carlsson, L.; Wegner, J.; Ceulemans, H.; Georgiev, I.; Jeliazkov, V.; Kochev, N.; Ashby, T. J.; Chen, H. ExCAPE-DB: An Integrated Large Scale Dataset Facilitating Big Data Analysis in Chemogenomics. *J. Cheminf.* **2017**, *9*, 17.

(27) Jenkins, J. L.; Glick, M.; Davies, J. W. A 3D Similarity Method for Scaffold Hopping from Known Drugs or Natural Ligands to New Chemotypes. *J. Med. Chem.* **2004**, *47*, 6144−6159.

(28) Jenkins, J. L. Feature Point Pharmacophores (FEPOPS). In *Scaffold Hopping in Medicinal Chemistry*; Methods and Principles in Medicinal Chemistry; Brown, N., Ed.; Wiley-VCH Verlag GmbH & Co. KGaA: Weinheim, Germany, 2013; pp 155−174.

(29) Schulz-Gasch, T.; Schärfer, C.; Guba, W.; Rarey, M. TFD: Torsion Fingerprints as a New Measure to Compare Small Molecule Conformations. *J. Chem. Inf. Model.* **2012**, *52*, 1499−1512.

(30) Mason, J. S.; Morize, I.; Menard, P. R.; Cheney, D. L.; Hulme, C.; Labaudiniere, R. F. New 4-Point Pharmacophore Method for Molecular Similarity and Diversity Applications: Overview of the Method and Applications, Including a Novel Approach to the Design of Combinatorial Libraries Containing Privileged Substructures. *J. Med. Chem.* **1999**, *42*, 3251−3264.

(31) Pickett, S. D.; Mason, J. S.; McLay, I. M. Diversity Profiling and Design Using 3D Pharmacophores: Pharmacophore-Derived Queries (PDQ). *J. Chem. Inf. Comput. Sci.* **1996**, *36*, 1214−1223.

(32) Sterling, T.; Irwin, J. J. ZINC 15–Ligand Discovery for Everyone. *J. Chem. Inf. Model.* **2015**, *55*, 2324−2337.

(33) Kearsley, S. K.; Sallamack, S.; Fluder, E. M.; Andose, J. D.; Mosley, R. T.; Sheridan, R. P. Chemical Similarity Using Physiochemical Property Descriptors. *J. Chem. Inf. Comput. Sci.* **1996**, *36*, 118−127.

(34) Awale, M.; Jin, X.; Reymond, J.-L. Stereoselective Virtual Screening of the ZINC Database Using Atom Pair 3D-Fingerprints. *J. Cheminf.* **2015**, *7*, 3.

(35) Rogers, D.; Hahn, M. Extended-Connectivity Fingerprints. *J. Chem. Inf. Model.* **2010**, *50*, 742−754.

(36) Morgan, H. L. The Generation of a Unique Machine Description for Chemical Structures-A Technique Developed at Chemical Abstracts Service. *J. Chem. Doc.* **1965**, *5*, 107−113.

(37) Barelier, S.; Sterling, T.; O'Meara, M. J.; Shoichet, B. K. The Recognition of Identical Ligands by Unrelated Proteins. *ACS Chem. Biol.* **2015**, *10*, 2772−2784.

(38) Ebejer, J.-P.; Morris, G. M.; Deane, C. M. Freely Available Conformer Generation Methods: How Good Are They? *J. Chem. Inf. Model.* **2012**, *52*, 1146−1158.

(39) Hert, J.; Willett, P.; Wilton, D. J.; Acklin, P.; Azzaoui, K.; Jacoby, E.; Schuffenhauer, A. Comparison of Fingerprint-Based Methods for Virtual Screening Using Multiple Bioactive Reference Structures. *J. Chem. Inf. Comput. Sci.* **2004**, *44*, 1177−1185.

(40) DeGraw, A. J.; Keiser, M. J.; Ochocki, J. D.; Shoichet, B. K.; Distefano, M. D. Prediction and Evaluation of Protein Farnesyltransferase Inhibition by Commercial Drugs. *J. Med. Chem.* **2010**, *53*, 2464−2471.

(41) Yee, S. W.; Lin, L.; Merski, M.; Keiser, M. J.; Gupta, A.; Zhang, Y.; Chien, H.-C.; Shoichet, B. K.; Giacomini, K. M. Prediction and Validation of Enzyme and Transporter Off-Targets for Metformin. *J. Pharmacokinet. Pharmacodyn.* **2015**, *42*, 463−475.

(42) Laggner, C.; Kokel, D.; Setola, V.; Tolia, A.; Lin, H.; Irwin, J. J.; Keiser, M. J.; Cheung, C. Y. J.; Minor, D. L.; Roth, B. L.; Peterson, R. T.; Shoichet, B. K. Chemical Informatics and Target Identification in a Zebrafish Phenotypic Screen. *Nat. Chem. Biol.* **2011**, *8*, 144−146.

(43) Lemieux, G. A.; Keiser, M. J.; Sassano, M. F.; Laggner, C.; Mayer, F.; Bainton, R. J.; Werb, Z.; Roth, B. L.; Shoichet, B. K.; Ashrafi, K. In Silico Molecular Comparisons of C. Elegans and Mammalian Pharmacology Identify Distinct Targets That Regulate Feeding. *PLoS Biol.* **2013**, *11*, e1001712.

(44) Bruni, G.; Rennekamp, A. J.; Velenich, A.; McCarroll, M.; Gendelev, L.; Fertsch, E.; Taylor, J.; Lakhani, P.; Lensen, D.; Evron, T.; Lorello, P. J.; Huang, X.-P.; Kolczewski, S.; Carey, G.; Caldarone, B. J.; Prinssen, E.; Roth, B. L.; Keiser, M. J.; Peterson, R. T.; Kokel, D. Zebrafish Behavioral Profiling Identifies Multitarget Antipsychotic-like Compounds. *Nat. Chem. Biol.* **2016**, *12*, 559−566.

(45) Lounkine, E.; Keiser, M. J.; Whitebread, S.; Mikhailov, D.; Hamon, J.; Jenkins, J. L.; Lavan, P.; Weber, E.; Doak, A. K.; Côté, S.; Shoichet, B. K.; Urban, L. Large-Scale Prediction and Testing of Drug Activity on Side-Effect Targets. *Nature* **2012**, *486*, 361−367.

(46) Lorberbaum, T.; Nasir, M.; Keiser, M. J.; Vilar, S.; Hripcsak, G.; Tatonetti, N. P. Systems Pharmacology Augments Drug Safety Surveillance. *Clin. Pharmacol. Ther.* **2015**, *97*, 151−158.

(47) Saito, T.; Rehmsmeier, M. The Precision-Recall Plot Is More Informative than the ROC Plot When Evaluating Binary Classifiers on Imbalanced Datasets. *PLoS One* **2015**, *10*, e0118432.

(48) Snoek, J.; Larochelle, H.; Adams, R. P. Practical Bayesian Optimization of Machine Learning Algorithms. *Neural Information Processing Systems Conference, Lake Tahoe, NV, December 3−8, 2012*; 2012.

(49) Froestl, W.; Mickel, S. J.; Hall, R. G.; von Sprecher, G.; Strub, D.; Baumann, P. A.; Brugger, F.; Gentsch, C.; Jaekel, J.; Olpe, H. R.; Riha, G.; Vassout, A.; Waldmeier, P. C.; Bittiger, H. Phosphinic Acid

Analogues of GABA. 1. New Potent and Selective GABAB Agonists. *J. Med. Chem.* **1995**, *38*, 3297−3312.

(50) Moormann, A. E.; Metz, S.; Toth, M. V.; Moore, W. M.; Jerome, G.; Kornmeier, C.; Manning, P.; Hansen, D. W.; Pitzele, B. S.; Webber, R. K. Selective Heterocyclic Amidine Inhibitors of Human Inducible Nitric Oxide Synthase. *Bioorg. Med. Chem. Lett.* **2001**, *11*, 2651−2653.

(51) Shankaran, K.; Donnelly, K. L.; Shah, S. K.; Guthikonda, R. N.; MacCoss, M.; Humes, J. L.; Pacholok, S. G.; Grant, S. K.; Kelly, T. M.; Wong, K. K. Evaluation of Pyrrolidin-2-Imines and 1,3-Thiazolidin-2-Imines as Inhibitors of Nitric Oxide Synthase. *Bioorg. Med. Chem. Lett.* **2004**, *14*, 4539−4544.

(52) Ponticello, G. S.; Freedman, M. B.; Habecker, C. N.; Lyle, P. A.; Schwam, H.; Varga, S. L.; Christy, M. E.; Randall, W. C.; Baldwin, J. J. Thienothiopyran-2-Sulfonamides: A Novel Class of Water-Soluble Carbonic Anhydrase Inhibitors. *J. Med. Chem.* **1987**, *30*, 591−597.

(53) Shankaran, K.; Donnelly, K. L.; Shah, S. K.; Caldwell, C. G.; Chen, P.; Hagmann, W. K.; Maccoss, M.; Humes, J. L.; Pacholok, S. G.; Kelly, T. M.; Grant, S. K.; Wong, K. K. Synthesis of Analogs of (1,4)-3- and 5-Imino Oxazepane, Thiazepane, and Diazepane as Inhibitors of Nitric Oxide Synthases. *Bioorg. Med. Chem. Lett.* **2004**, *14*, 5907−5911.

(54) Moore, W. M.; Webber, R. K.; Fok, K. F.; Jerome, G. M.; Connor, J. R.; Manning, P. T.; Wyatt, P. S.; Misko, T. P.; Tjoeng, F. S.; Currie, M. G. 2-Iminopiperidine and Other 2-Iminoazaheterocycles as Potent Inhibitors of Human Nitric Oxide Synthase Isoforms. *J. Med. Chem.* **1996**, *39*, 669−672.

(55) Monn, J. A.; Massey, S. M.; Valli, M. J.; Henry, S. S.; Stephenson, G. A.; Bures, M.; Hérin, M.; Catlow, J.; Giera, D.; Wright, R. A.; Johnson, B. G.; Andis, S. L.; Kingston, A.; Schoepp, D. D. Synthesis and Metabotropic Glutamate Receptor Activity of S-Oxidized Variants of (−)-4-Amino-2-Thiabicyclo-[3.1.0]Hexane-4,6-Dicarboxylate: Identification of Potent, Selective, and Orally Bioavailable Agonists for MGlu2/3 Receptors. *J. Med. Chem.* **2007**, *50*, 233−240.

(56) Nersesian, D. L.; Black, L. A.; Miller, T. R.; Vortherms, T. A.; Esbenshade, T. A.; Hancock, A. A.; Cowart, M. D. In Vitro SAR of Pyrrolidine-Containing Histamine H3 Receptor Antagonists: Trends across Multiple Chemical Series. *Bioorg. Med. Chem. Lett.* **2008**, *18*, 355−359.

(57) Rogers, G. A.; Parsons, S. M.; Anderson, D. C.; Nilsson, L. M.; Bahr, B. A.; Kornreich, W. D.; Kaufman, R.; Jacobs, R. S.; Kirtman, B. Synthesis, in Vitro Acetylcholine-Storage-Blocking Activities, and Biological Properties of Derivatives and Analogues of Trans-2-(4-Phenylpiperidino)Cyclohexanol (Vesamicol). *J. Med. Chem.* **1989**, *32*, 1217−1230.

(58) Röver, S.; Wichmann, J.; Jenck, F.; Adam, G.; Cesura, A. M. ORL1 Receptor Ligands: Structure-Activity Relationships of 8-Cycloalkyl-1-Phenyl-1,3,8-Triaza-Spiro[4.5]Decan-4-Ones. *Bioorg. Med. Chem. Lett.* **2000**, *10*, 831−834.

(59) Kaltenbach, R. F.; Nugiel, D. A.; Lam, P. Y.; Klabe, R. M.; Seitz, S. P. Stereoisomers of Cyclic Urea HIV-1 Protease Inhibitors: Synthesis and Binding Affinities. *J. Med. Chem.* **1998**, *41*, 5113−5117.

(60) Lam, P. Y.; Ru, Y.; Jadhav, P. K.; Aldrich, P. E.; DeLucca, G. V.; Eyermann, C. J.; Chang, C. H.; Emmett, G.; Holler, E. R.; Daneker, W. F.; Li, L.; Confalone, P. N.; McHugh, R. J.; Han, Q.; Li, R.; Markwalder, J. A.; Seitz, S. P.; Sharpe, T. R.; Bacheler, L. T.; Rayner, M. M.; Klabe, R. M.; Shum, L.; Winslow, D. L.; Kornhauser, D. M.; Jackson, D. A.; Erickson-Viitanen, S.; Hodge, C. N. Cyclic HIV Protease Inhibitors: Synthesis, Conformational Analysis, P2/P2′ Structure-Activity Relationship, and Molecular Recognition of Cyclic Ureas. *J. Med. Chem.* **1996**, *39*, 3514−3525.

(61) Xu, B.; Feng, Y.; Cheng, H.; Song, Y.; Lv, B.; Wu, Y.; Wang, C.; Li, S.; Xu, M.; Du, J.; Peng, K.; Dong, J.; Zhang, W.; Zhang, T.; Zhu, L.; Ding, H.; Sheng, Z.; Welihinda, A.; Roberge, J. Y.; Seed, B.; Chen, Y. C-Aryl Glucosides Substituted at the 4′-Position as Potent and Selective Renal Sodium-Dependent Glucose Co-Transporter 2 (SGLT2) Inhibitors for the Treatment of Type 2 Diabetes. *Bioorg. Med. Chem. Lett.* **2011**, *21*, 4465−4470.

(62) Xu, G.; Lv, B.; Roberge, J. Y.; Xu, B.; Du, J.; Dong, J.; Chen, Y.; Peng, K.; Zhang, L.; Tang, X.; Feng, Y.; Xu, M.; Fu, W.; Zhang, W.; Zhu, L.; Deng, Z.; Sheng, Z.; Welihinda, A.; Sun, X. Design, Synthesis, and Biological Evaluation of Deuterated C-Aryl Glycoside as a Potent and Long-Acting Renal Sodium-Dependent Glucose Cotransporter 2 Inhibitor for the Treatment of Type 2 Diabetes. *J. Med. Chem.* **2014**, *57*, 1236−1251.

(63) Horii, S.; Fukase, H.; Matsuo, T.; Kameda, Y.; Asano, N.; Matsui, K. Synthesis and Alpha-D-Glucosidase Inhibitory Activity of N-Substituted Valiolamine Derivatives as Potential Oral Antidiabetic Agents. *J. Med. Chem.* **1986**, *29*, 1038−1046.

(64) Gao, L.-J.; Waelbroeck, M.; Hofman, S.; Van Haver, D.; Milanesio, M.; Viterbo, D.; De Clercq, P. J. Synthesis and Affinity Studies of Himbacine Derived Muscarinic Receptor Antagonists. *Bioorg. Med. Chem. Lett.* **2002**, *12*, 1909−1912.

(65) de Costa, B. R.; Rice, K. C.; Bowen, W. D.; Thurkauf, A.; Rothman, R. B.; Band, L.; Jacobson, A. E.; Radesca, L.; Contreras, P. C.; Gray, N. M.; Daly, I.; Iyengar, S.; Finn, D. T.; Vazirani, S.; Walker, J. M. Synthesis and Evaluation of N-Substituted Cis-N-Methyl-2-(1-Pyrrolidinyl)Cyclohexylamines as High Affinity Sigma Receptor Ligands. Identification of a New Class of Highly Potent and Selective Sigma Receptor Probes. *J. Med. Chem.* **1990**, *33*, 3100−3110.

(66) Besnard, J.; Ruda, G. F.; Setola, V.; Abecassis, K.; Rodriguiz, R. M.; Huang, X.-P.; Norval, S.; Sassano, M. F.; Shin, A. I.; Webster, L. A.; Simeons, F. R. C.; Stojanovski, L.; Prat, A.; Seidah, N. G.; Constam, D. B.; Bickerton, G. R.; Read, K. D.; Wetsel, W. C.; Gilbert, I. H.; Roth, B. L.; Hopkins, A. L. Automated Design of Ligands to Polypharmacological Profiles. *Nature* **2012**, *492*, 215−220.

(67) Kanehisa, M.; Furumichi, M.; Tanabe, M.; Sato, Y.; Morishima, K. KEGG: New Perspectives on Genomes, Pathways, Diseases and Drugs. *Nucleic Acids Res.* **2017**, *45*, D353−D361.

(68) Kanehisa, M.; Sato, Y.; Kawashima, M.; Furumichi, M.; Tanabe, M. KEGG as a Reference Resource for Gene and Protein Annotation. *Nucleic Acids Res.* **2016**, *44*, D457−D462.

(69) Kanehisa, M.; Goto, S. KEGG: Kyoto Encyclopedia of Genes and Genomes. *Nucleic Acids Res.* **2000**, *28*, 27−30.

(70) Hopkins, A. L.; Keserü, G. M.; Leeson, P. D.; Rees, D. C.; Reynolds, C. H. The Role of Ligand Efficiency Metrics in Drug Discovery. *Nat. Rev. Drug Discovery* **2014**, *13*, 105−121.

(71) Schlicker, E.; Werner, U.; Hamon, M.; Gozlan, H.; Nickel, B.; Szelenyi, I.; Göthert, M. Anpirtoline, a Novel, Highly Potent 5-HT1B Receptor Agonist with Antinociceptive/Antidepressant-like Actions in Rodents. *Br. J. Pharmacol.* **1992**, *105*, 732−738.

(72) Metzenauer, P.; Barnes, N. M.; Costall, B.; Gozlan, H.; Hamon, M.; Kelly, M. E.; Murphy, D. A.; Naylor, R. J. Anxiolytic-like Actions of Anpirtoline in a Mouse Light-Dark Aversion Paradigm. *NeuroReport* **1992**, *3*, 527−529.

(73) Moore, P. A. Local Anesthesia and Narcotic Drug Interaction in Pediatric Dentistry. *Anesth. Prog.* **1988**, *35*, 17.

(74) Barnea, G.; Strapps, W.; Herrada, G.; Berman, Y.; Ong, J.; Kloss, B.; Axel, R.; Lee, K. J. The Genetic Design of Signaling Cascades to Record Receptor Activation. *Proc. Natl. Acad. Sci. U. S. A.* **2008**, *105*, 64−69.

(75) Kroeze, W. K.; Sassano, M. F.; Huang, X.-P.; Lansu, K.; McCorvy, J. D.; Giguère, P. M.; Sciaky, N.; Roth, B. L. PRESTO-Tango as an Open-Source Resource for Interrogation of the Druggable Human GPCRome. *Nat. Struct. Mol. Biol.* **2015**, *22*, 362−369.

(76) Gentry, P. R.; Kokubo, M.; Bridges, T. M.; Cho, H. P.; Smith, E.; Chase, P.; Hodder, P. S.; Utley, T. J.; Rajapakse, A.; Byers, F.; Niswender, C. M.; Morrison, R. D.; Daniels, J. S.; Wood, M. R.; Conn, P. J.; Lindsley, C. W. Discovery, Synthesis and Characterization of a Highly Muscarinic Acetylcholine Receptor (MAChR)-Selective M5-Orthosteric Antagonist, VU0488130 (ML381): A Novel Molecular Probe. *ChemMedChem* **2014**, *9*, 1677−1682.

(77) Cleves, A. E.; Jain, A. N. Effects of Inductive Bias on Computational Evaluations of Ligand-Based Modeling and on Drug Discovery. *J. Comput.-Aided Mol. Des.* **2008**, *22*, 147−159.

(78) Fink-Jensen, A.; Fedorova, I.; Wörtwein, G.; Woldbye, D. P. D.; Rasmussen, T.; Thomsen, M.; Bolwig, T. G.; Knitowski, K. M.; McKinzie, D. L.; Yamada, M.; Wess, J.; Basile, A. Role for M5Muscarinic Acetylcholine Receptors in Cocaine Addiction. *J. Neurosci. Res.* **2003**, *74*, 91−96.

(79) Basile, A. S.; Fedorova, I.; Zapata, A.; Liu, X.; Shippenberg, T.; Duttaroy, A.; Yamada, M.; Wess, J. Deletion of the M5Muscarinic Acetylcholine Receptor Attenuates Morphine Reinforcement and Withdrawal but Not Morphine Analgesia. *Proc. Natl. Acad. Sci. U. S. A.* **2002**, *99*, 11452−11457.

(80) Yamada, M.; Lamping, K. G.; Duttaroy, A.; Zhang, W.; Cui, Y.; Bymaster, F. P.; McKinzie, D. L.; Felder, C. C.; Deng, C. X.; Faraci, F. M.; Wess, J. Cholinergic Dilation of Cerebral Blood Vessels Is Abolished in M(5) Muscarinic Acetylcholine Receptor Knockout Mice. *Proc. Natl. Acad. Sci. U. S. A.* **2001**, *98*, 14096−14101.

(81) Chen, D. T. Alphaprodine HCl: Characteristics. *Pediatric Dentistry* **1982**, *4*, 158−163.

(82) Bird, P. Compositions and Methods for Treating Psychiatric Disorders. US20160000815A1, January 7, 2016.

(83) Bird, P. Treatment of ADHD. US8957099B2, February 17, 2015.

(84) Fleisher, C.; McGough, J. Sofinicline: A Novel Nicotinic Acetylcholine Receptor Agonist in the Treatment of Attention-Deficit/Hyperactivity Disorder. *Expert Opin. Invest. Drugs* **2014**, *23*, 1157−1163.

(85) Kent, L.; Middle, F.; Hawi, Z.; Fitzgerald, M.; Gill, M.; Feehan, C.; Craddock, N. Nicotinic Acetylcholine Receptor Alpha4 Subunit Gene Polymorphism and Attention Deficit Hyperactivity Disorder. *Psychiatr. Genet.* **2001**, *11*, 37−40.

(86) Salas, R.; Cook, K. D.; Bassetto, L.; De Biasi, M. The Alpha3 and Beta4 Nicotinic Acetylcholine Receptor Subunits Are Necessary for Nicotine-Induced Seizures and Hypolocomotion in Mice. *Neuropharmacology* **2004**, *47*, 401−407.

(87) Zaveri, N.; Jiang, F.; Olsen, C.; Polgar, W.; Toll, L. Novel A3β4 Nicotinic Acetylcholine Receptor-Selective Ligands. Discovery, Structure-Activity Studies, and Pharmacological Evaluation. *J. Med. Chem.* **2010**, *53*, 8187−8191.

(88) Allen, F. H. The Cambridge Structural Database: A Quarter of a Million Crystal Structures and Rising. *Acta Crystallogr., Sect. B: Struct. Sci.* **2002**, *58*, 380−388.

(89) Kellenberger, E.; Muller, P.; Schalon, C.; Bret, G.; Foata, N.; Rognan, D. Sc-PDB: An Annotated Database of Druggable Binding Sites from the Protein Data Bank. *J. Chem. Inf. Model.* **2006**, *46*, 717−727.

(90) Halgren, T. A. Merck Molecular Force Field. I. Basis, Form, Scope, Parameterization, and Performance of MMFF94. *J. Comput. Chem.* **1996**, *17*, 490−519.

(91) González, M. A. Force Fields and Molecular Dynamics Simulations. *JDN* **2011**, *12*, 169−200.

(92) Rappe, A. K.; Casewit, C. J.; Colwell, K. S.; Goddard, W. A.; Skiff, W. M. UFF, a Full Periodic Table Force Field for Molecular Mechanics and Molecular Dynamics Simulations. *J. Am. Chem. Soc.* **1992**, *114*, 10024−10035.

(93) *RDKit: Open-Source Cheminformatics*; GitHub, 2016; http://www.rdkit.org (accessed Feb 8, 2016).

(94) *Marvin*; ChemAxon, 2015.

(95) Appleby, A. *MurmurHash3*; GitHub, 2016; https://github.com/aappleby/smhasher (accessed Feb 8, 2016).

(96) Triballeau, N.; Acher, F.; Brabet, I.; Pin, J.-P.; Bertrand, H.-O. Virtual Screening Workflow Development Guided by the "Receiver Operating Characteristic" Curve Approach. Application to High-Throughput Docking on Metabotropic Glutamate Receptor Subtype 4. *J. Med. Chem.* **2005**, *48*, 2534−2547.

(97) Srivastava, N.; Hinton, G.; Krizhevsky, A.; Sutskever, I.; Salakhutdinov, R. Dropout: A Simple Way to Prevent Neural Networks from Overfitting. *J. Mach. Learn. Res.* **2014**, *15*, 1929−1958.

(98) Maas, A. L.; Hannun, A. Y.; Ng, A. Y. Rectifier Nonlinearities Improve Neural Network Acoustic Models. In *Proceedings of the 30th International Conference on Machine Learning, Atlanta, GA, June 16−21, 2013*; 2013.

(99) Desaphy, J.; Bret, G.; Rognan, D.; Kellenberger, E. Sc-PDB: A 3D-Database of Ligandable Binding Sites–10 Years On. *Nucleic Acids Res.* **2015**, *43*, D399−404.

(100) Xiao, Y.; Meyer, E. L.; Thompson, J. M.; Surin, A.; Wroblewski, J.; Kellar, K. J. Rat Alpha3/Beta4 Subtype of Neuronal Nicotinic Acetylcholine Receptor Stably Expressed in a Transfected Cell Line: Pharmacology of Ligand Binding and Function. *Mol. Pharmacol.* **1998**, *54*, 322−333.

(101) Xiao, Y.; Fan, H.; Musachio, J. L.; Wei, Z.-L.; Chellappan, S. K.; Kozikowski, A. P.; Kellar, K. J. Sazetidine-A, a Novel Ligand That Desensitizes Alpha4beta2 Nicotinic Acetylcholine Receptors without Activating Them. *Mol. Pharmacol.* **2006**, *70*, 1454−1460.

(102) Kuntz, I. D.; Chen, K.; Sharp, K. A.; Kollman, P. A. The Maximal Affinity of Ligands. *Proc. Natl. Acad. Sci. U. S. A.* **1999**, *96*, 9997−10002.